Appendix A

In the main body of this book we have described particle and nuclear physics and the underlying interactions concisely and in context. We have here and there elucidated the basic principles and methods of the experiments that have led us to this knowledge. We now want to briefly describe the individual tools of experimental physics – the particle accelerators and detectors – whose invention and development have often been a sine qua non for the discoveries discussed here. More detailed discussions may be found in the literature [4, 7, 11, 15–17].

A.1 Accelerators

Particle accelerators provide us with different types of particle beams whose energies (at the time of writing) can be anything up to a few TeV (10^6 MeV). These beams serve on the one hand as "sources" of energy which if used to bombard nuclei can generate a variety of excited states or indeed new particles. On the other hand they can act as "probes" with which we may investigate the structure of the target particle.

The most important quantity, whether we want to generate new particles or excite a system into a higher state, is the centre-of-mass energy $\sqrt{s}$ of the reaction under investigation. In the reaction of a beam particle a with total energy E_a with a target particle b which is at rest this is

$$\sqrt{s} = \sqrt{2E_\mathrm{a}m_\mathrm{b}c^2 + (m_\mathrm{a}^2 + m_\mathrm{b}^2)c^4}\,. \tag{A.1}$$

In high energy experiments where the particle masses may be neglected in comparison to the beam energy this simplifies to

$$\sqrt{s} = \sqrt{2E_\mathrm{a}m_\mathrm{b}c^2}\,. \tag{A.2}$$

B. Povh et al., *Particles and Nuclei*, Graduate Texts in Physics,
DOI 10.1007/978-3-662-46321-5

The centre-of-mass energy for a stationary target only, we see, grows with the square root of the beam particle's energy.

If a beam particle with momentum p is used to investigate the structure of a stationary target, then the best possible resolution is characterised by its reduced de Broglie wavelength $\lambda\!\!\!^{-} = \hbar/p$. This is related to the energy E through (4.1).

All accelerators essentially consist of the following: a particle source, a structure to actually do the accelerating and an evacuated beam pipe. It should also be possible to focus and deflect the particle beam. The accelerating principle is always the same: charged particles are accelerated if they are exposed to an electric field. A particle with charge Ze which traverses a potential difference U receives an amount of energy, $E = Ze\,U$. In the following we wish to briefly present the three most important types of accelerators.

Electrostatic accelerators In these accelerators the relation $E = Ze\,U$ is directly exploited. The main components of an electrostatic accelerator are a high voltage generator, a terminal and an evacuated beam pipe. In the most common sort, the *Van de Graaff accelerator*, the terminal is usually a metallic sphere which acts as a capacitor with capacitance C. The terminal is charged by a rotating, insulated band and this creates a high electric field. From a grounded potential positive charges are brought onto the band and then stripped off onto the terminal. The entire set up is placed inside an grounded tank which is filled with an insulating gas (e.g., SF_6) to prevent premature discharge. The voltage $U = Q/C$ which may be built up in this way can be as much as 15 MV. Positive ions, produced in an ion source, at the terminal potential now traverse inside the beam pipe the entire potential difference between the terminal and the tank. Protons can in this way reach kinetic energies up to 15 MeV.

Energies twice as high may be attained in tandem Van de Graaff accelerators (Fig. A.1). Here the accelerating potential is used twice over. Negative ions are first produced at ground potential and then accelerated along a beam pipe towards the terminal. A thin foil, or similar, placed there strips some of the electrons off the ions and leaves them positively charged. The accelerating voltage now enters the game again and protons may in this way attain kinetic energies of up to 30 MeV. Heavy ions may lose several electrons at once and consequently reach even higher kinetic energies.

Van de Graaff accelerators can provide reliable, continuous particle beams with currents of up to 100 μA. They are very important workhorses for nuclear physics. Protons and both light and heavy ions may be accelerated in them up to energies at which nuclear reactions and nuclear spectroscopy may be systematically investigated.

Linear accelerators GeV-type energies may only be attained by repeatedly accelerating the particle. Linear accelerators, which are based upon this principle, are made up of many accelerating tubes laid out in a straight line and the particles progress along their central axis. Every pair of neighbouring tubes have oppositely arranged potentials such that the particles between them are accelerated, while the interior of the tubes is essentially field free (Wideröe type). A high frequency

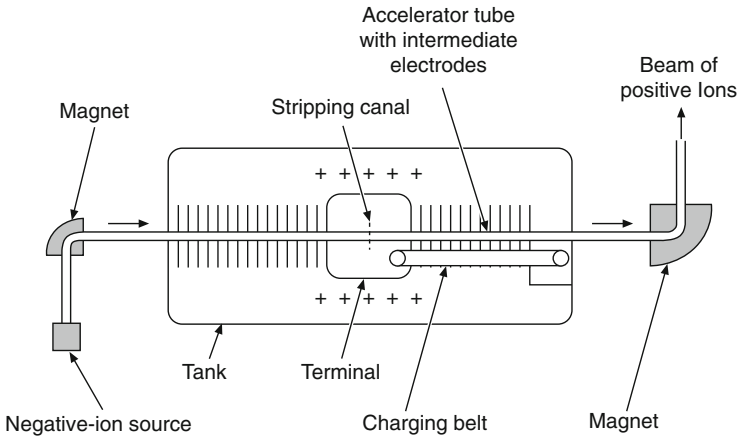

Fig. A.1 Sketch of a tandem Van de Graaff accelerator. Negative ions are accelerated from the left towards the terminal where some of their electrons are stripped off and they become positively charged. This causes them to now be accelerated away from the terminal and the potential difference between the terminal and the tank is traversed for a second time

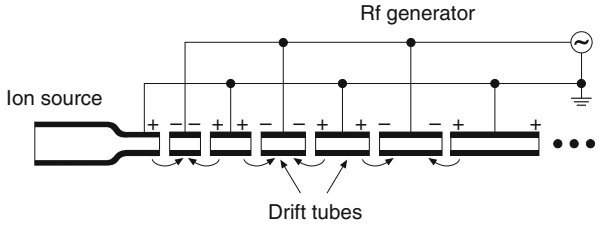

Fig. A.2 Sketch of the fundamentals of a (Wideröe type) linear accelerator. The potentials of the tubes shown are for one particular moment in time. The particles are accelerated from the source to the first drift tube. The lengths L_i of the tubes and the generator frequency ω must be adjusted to each other so that we have $L_i = v_i \pi/\omega$ where v_i is the particle velocity at the ith tube. This depends both upon the generator voltage and the type of particle being accelerated

generator changes the potentials with a period such that the particles between the tubes always feel an accelerating force. After passing through n tubes the particles will have kinetic energy $E = nZe\,U$. Such accelerators cannot produce continuous particle beams; they accelerate packets of particles which are in phase with the generator frequency.

Since the generator frequency is fixed, the lengths of the various stages need to be adjusted to fit the speed of the particles as they pass through (Fig. A.2). If we have an electron beam this last subtlety is only relevant for the first few acceleration steps, since the small electron mass means that their velocity is very soon nearly equal to the speed of light. On the other hand the tube lengths generally need to be continually altered along the entire length of proton linear accelerators. The final

energy of a linear accelerator is determined by the number of tubes and the maximal potential difference between them.

At present the largest linear accelerator in the world, where many important experiments on deep inelastic scattering off nucleons have been carried out, was the roughly 3 km long electron linear accelerator at the Stanford Linear Accelerator Center (SLAC). Here electrons passed through around 100,000 accelerating stages to reach energies of about 50 GeV.

Synchrotrons While particles pass through each stage of a linear accelerator just once, synchrotrons, which have a circular form, may be used to accelerate particles to high energies by passing them many times through the same accelerating structures.

The particles are kept on their circular orbits by magnetic fields. The accelerating stages are mostly only placed at a few positions upon the circuit. The principle of the synchrotron is to synchronously change the generator frequency ω of the accelerating stages together with the magnetic field B in such a way that the particles, whose orbital frequencies and momenta p are increasing as a result of the acceleration, always feel an accelerating force and are simultaneously kept on their assigned orbits inside the vacuum pipe. This means that the following constraints must be simultaneously fulfilled:

$$\omega = n \cdot \frac{c}{R} \cdot \frac{p\,c}{E} \qquad n = \text{positive integer} \tag{A.3}$$

$$B = \frac{p}{Ze\,R}\,, \tag{A.4}$$

where R is the radius of curvature of the synchrotron ring. Technical limitations upon the B and ω available mean that one has to inject preaccelerated particles into synchrotron rings whereupon they can be brought up to their preassigned final energy. Linear accelerators or smaller synchrotrons are used in the preacceleration stage. Synchrotrons also only produce packets of particles and do not deliver continuous beams.

High particle intensities require well focused beams close to the ideal orbit. Focusing is also of great importance in the transport of the beam from the preaccelerator to the main stage and from there to the experiment (injection and extraction). Magnetic lenses, made from quadrupole magnets, are used to focus the beam in high energy accelerators. The field of a quadrupole magnet focuses charged particles in one plane on its central axis and defocuses them on the other plane perpendicular to it. An overall focusing in both planes may be achieved by putting a second quadrupole magnet, whose poles are rotated relative to those of the first one through 90°, after the first magnet. This principle of *strong focusing* is similar to the optical combination of thin diverging and converging lenses which always effectively focuses. Figure A.3 depicts the essentials of a synchrotron and the focusing effects of such quadrupole doublets.

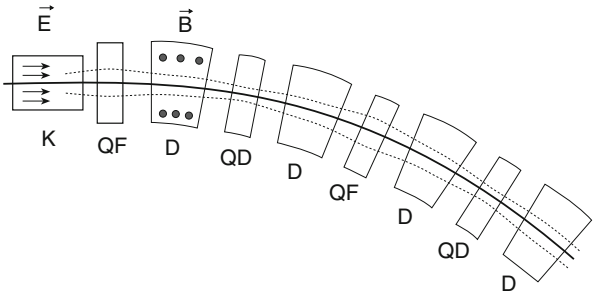

Fig. A.3 Section (to scale) of a synchrotron from above. The essential accelerating and magnetic structures are shown together with the beam pipe (*continuous line*). High frequency accelerator tubes (K) are usually only placed at a few positions around the synchrotron. The fields of the dipole magnets (D), which keep the particles on their circular paths, are perpendicular to the page. Pairs of quadrupole magnets form doublets which focus the beam. This is indicated by the *dotted lines* which (exaggeratedly) show the shape of the beam envelope. The quadrupoles marked QF have a focusing effect in the plane of the page and the QD quadrupoles a defocusing effect

Particles accelerated in synchrotrons lose some of their energy to *synchrotron radiation*. This refers to the emission of photons by any charged particle which is forced onto a circular path and is thus radially accelerated. The energy lost to synchrotron radiation must be compensated by the accelerating stages. This loss is for highly relativistic particles

$$-\Delta E = \frac{4\pi\alpha\hbar c}{3R}\beta^3\gamma^4\,, \qquad \text{where} \quad \beta = \frac{v}{c} \approx 1 \quad \text{and} \quad \gamma = \frac{E}{mc^2}\,, \tag{A.5}$$

per orbit – it increases in other words with the fourth power of the particle energy E. The mass dependence means that this rate of energy loss is about 10^{13} times larger for electrons than for protons of the same energy. The maximal energy in modern electron synchrotrons is thus about 100 GeV. Synchrotron radiation does not play an important role for proton beams. The limit on their final energy is set by the available field strengths of the dipole magnets which keep the protons in the orbit. Proton energies up to a few TeV may be achieved with superconducting magnets.

There are two types of experiment which use particles accelerated in synchrotrons. The beam may, after it has reached its final energy, be deflected out of the ring and led off towards a stationary target. Alternatively the beam may be stored in the synchrotron until it is either loosed upon a thin, internal target or collided with another beam.

Storage rings The centre-of-mass energy of a reaction involving a stationary target only grows with the square root of the beam energy (A.2). Much higher centre-of-mass energies may be obtained for the same beam energies if we employ colliding particle beams. The centre-of-mass energy for a head on collision of two particle beams with energy E is $\sqrt{s} = 2E$ – i.e., it increases linearly with the beam energy.

The particle density in particle beams, and hence the reaction rate for the collision of two beams, is very tiny; thus they need to be repeatedly collided in any experiment with reasonable event rates. High collision rates may, e.g., be obtained by continuously operating two linear accelerators and colliding the particle beams they produce. Another possibility is to store particle beams, which were accelerated in a synchrotron, at their final energy and at the accelerating stages just top up the energy they lose to synchrotron radiation. These stored particle beams may be then used for collision experiments.

Consider as an example the HERA ring at the Deutsche Elektronen-Synchrotron (German Electron Synchrotron, DESY) in Hamburg that was operated during the years 1992–2007. This was made up of two separate storage rings of the same diameter which run parallel to each other at about 1 m separation. Electrons were accelerated up to about 27.6 GeV and protons to about 920 GeV before storage. The beam tubes came together at two points, where the detectors were positioned, and the oppositely circling beams were allowed to collide there.

Construction is rather simpler if one wants to collide particles with their antiparticles (e.g., electrons and positrons or protons and antiprotons). In such cases only one storage ring is needed and these equal mass but oppositely charged particles can simultaneously run around the ring in opposite directions and may be brought to collision at various interaction points. Examples of these are the LEP ring (Large Electron Positron Ring) at CERN where electrons and positrons with energies up to 104.6 GeV collided and the Sp$\overline{\text{p}}$S (Super Proton Antiproton Synchrotron) where 310 GeV protons and antiprotons were brought violently together. Both of these machines were to be found at the European Nuclear Research Centre CERN near Geneva.

An example of a research complex of accelerators is shown in Fig. A.4; that of DESY. A total of seven preaccelerators service the DORIS and HERA storage rings where experiments with electrons, positrons and protons take place. Two preaccelerator stages are needed for the electron-positron ring DORIS where the beams each have a maximal energy of 5.6 GeV. Three such stages are required for the electron-proton ring HERA (27.6 GeV electrons and 920 GeV protons). DORIS also served as an source of intensive synchrotron radiation and was used as a research instrument in surface physics, chemistry, biology and medicine.

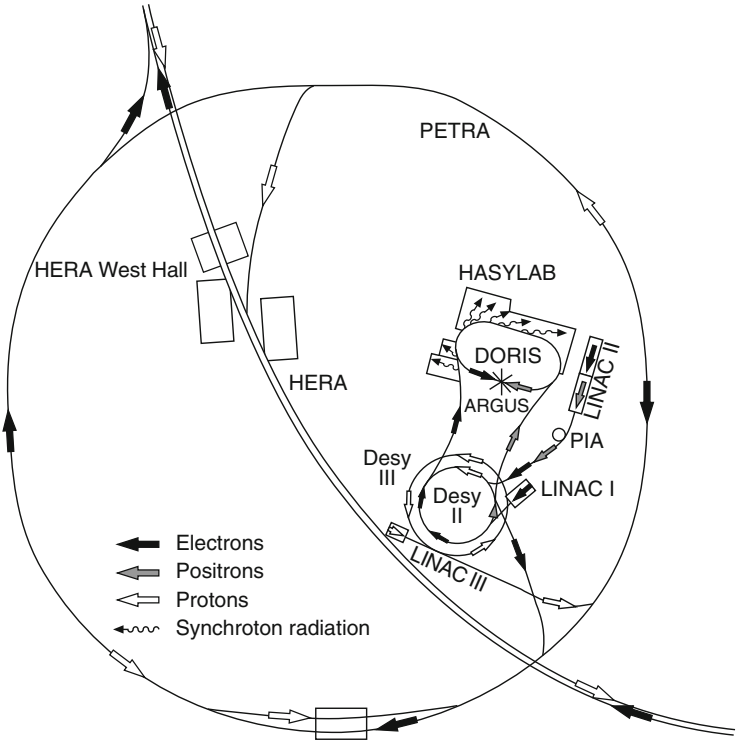

Fig. A.4 The accelerator complex at the German Electron Synchrotron, DESY, in Hamburg. The DORIS and HERA storage rings are serviced by a chain of preaccelerators. Electrons are accelerated up to 450 MeV in the LINAC I or LINAC II linear accelerators before being injected into the DESY II synchrotron, where they may reach up to 9 GeV. Thence they either pass into DORIS or the PETRA synchrotron. PETRA acts as a final preaccelerator for HERA and electron energies of up to 14 GeV may be attained there. Before HERA was commissioned PETRA worked as an electron-positron storage ring with a beam energy of up to 23.5 GeV. Positrons are produced with the help of electrons accelerated in LINAC II and are then accumulated in the PIA storage ring before their injection into DESY II where they are further accelerated and then led off to DORIS. Protons are accelerated in LINAC III up to 50 MeV and then preaccelerated in the proton synchrotron DESY III up to 7.5 GeV before being injected into PETRA. There they attain 40 GeV before being injected into HERA. The HERA ring, which is only partially shown here, has a circumference of 6,336 m, while the circumference of PETRA is 2,300 m and that of DESY II(III) is around 300 m (*Courtesy of DESY*)

A.2 Detectors

The construction and development of detectors for particle and nuclear physics has, as with accelerator physics, developed into an almost independent branch of science. The demands upon the quality and complexity of these detectors increase with the ever higher particle energies and currents involved. This has necessarily led to a strong specialisation among the detectors. There are now detectors to measure times,

particle positions, momenta and energies and to identify the particles involved. The principles underlying the detectors are mostly based upon the electromagnetic interactions of particles with matter, e.g., ionisation processes. We will therefore first briefly delineate these processes before showing how they are applied in the individual detectors.

Interaction of particles with matter If charged particles pass through matter they lose energy through collisions with the medium. A large part of this corresponds to interactions with the atomic electron clouds which lead to the atoms being excited or ionised. The energy lost to ionisation is described by the *Bethe-Bloch formula* [1, 2]. Approximately we have [12]

$$-\frac{\mathrm{d}E}{\mathrm{d}x} = \frac{4\pi}{m_\mathrm{e}c^2}\frac{nz^2}{\beta^2}\left(\frac{e^2}{4\pi\varepsilon_0}\right)^2\left[\ln\frac{2m_\mathrm{e}c^2\beta^2}{I\cdot(1-\beta^2)} - \beta^2\right], \tag{A.6}$$

where $\beta = v/c$, ze and v are the charge and speed of the particle, n is the electron density and I is the average excitation potential of the atoms (typically $16\,\mathrm{eV}\cdot Z^{0.9}$ for nuclear charge numbers $Z > 1$). The energy loss thus depends upon the charge and speed of the particle (Fig. A.5) but not upon its mass. It decreases for small velocities as $1/v^2$, reaches a minimum around $p/mc \approx 4$ and then increases only logarithmically for relativistic velocities. The energy loss to ionisation per length $\mathrm{d}x$ traversed normalised to the density ϱ of the matter at the ionisation minimum, and also for higher particle energies, is roughly $1/\varrho \cdot \mathrm{d}E/\mathrm{d}x \approx 2\,\mathrm{MeV}/(\mathrm{g\,cm^{-2}})$.

Electrons and positrons lose energy not just to ionisation but also to a further important process: *bremsstrahlung*. Electrons braking in the field of a nucleus radiate energy in the form of photons. This process strongly depends upon the material and the energy: it increases roughly linearly with energy and quadratically with the charge number Z of the medium. Above a critical energy E_c, which may

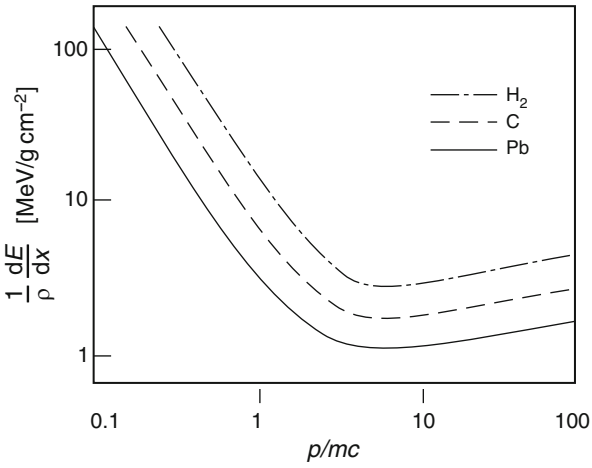

Fig. A.5 Rough sketch of the average energy loss of charged particles to ionisation processes in hydrogen, carbon and lead. The energy loss divided by the density of the material is plotted against $p/mc = \beta\gamma$ for the particle in a log-log plot. The specific energy loss is greater for lighter elements than for heavy ones

be coarsely parametrised by $E_c \approx 600\,\mathrm{MeV}/Z$, bremsstrahlung energy loss is more important for electrons than is ionisation. For such high energy electrons an important material parameter is the *radiation length* X_0. This describes the distance over which the electron energy decreases due to bremsstrahlung by a factor of e. High energy electrons are best absorbed in materials with high charge numbers Z, e.g., lead, where the radiation length is just 0.56 cm.

While charged particles traversing matter lose energy slowly to electromagnetic interactions before finally being absorbed, the interaction of a photon with matter takes place at a point. The intensity I of a photon beam therefore decreases exponentially with the thickness ℓ of the matter traversed:

$$I = I_0 \cdot \mathrm{e}^{-\mu \ell} \,. \tag{A.7}$$

The absorption coefficient μ depends upon the photon energy and the type of matter.

The interaction of photons with matter essentially takes place via one of three processes: the *photoelectric effect*, the *Compton effect* and *pair production*. These processes depend strongly upon the medium and the energy involved. The photoelectric effect dominates at low energies in the keV range, the Compton effect for energies from several 100 keV to a few MeV while in high energy experiments only pair production is of any importance. Here the photon is converted inside the nuclear field to an electron-positron pair. This is the dominant process above several MeV. In this energy range the photon can also be described by the radiation length X_0: the conversion length λ of a high energy photon is $\lambda = 9/7 \cdot X_0$. The energy dependence of these three processes in lead is illustrated in Fig. A.6.

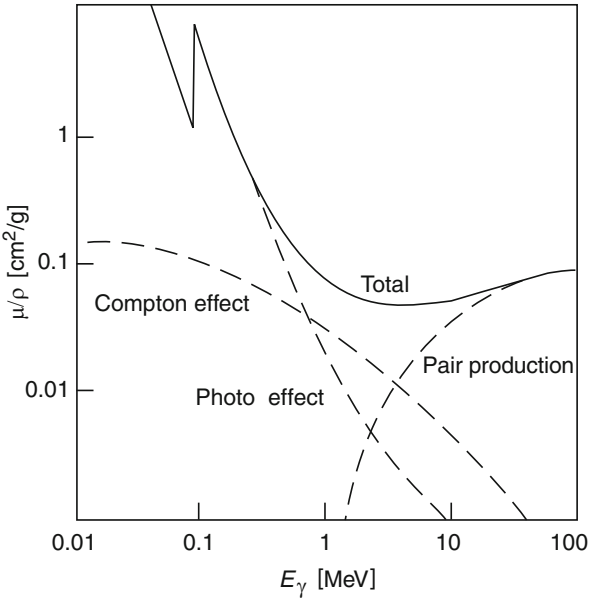

Fig. A.6 The photon absorption coefficient μ in lead divided by the density plotted against the photon energy. The *dashed lines* are the contributions of the individual processes; the photoelectric effect, the Compton effect and pair production. Above a few MeV pair production plays the dominant role

We wish to briefly mention two further processes which are useful in particle identification: the radiation of Cherenkov light and nuclear reactions. *Cherenkov radiation* is photon emission from charged particles that cross through a medium with a velocity greater than the speed of light in that medium. These photons are radiated in a cone with angle

$$\theta = \arccos \frac{1}{\beta\, n} \tag{A.8}$$

around the path of the charged particle (n is the refractive index of the medium). The energy loss to Cherenkov radiation is small compared to that through ionisation.

Nuclear reactions are important for detecting neutral hadrons such as neutrons that do not participate in any of the above processes. Possible reactions are nuclear fission and neutron capture (eV-keV range), elastic and inelastic scattering (MeV range) and hadron production (high energies).

Measuring positions The ability to measure the positions and momenta of particles is important in order to reconstruct the kinematics of reactions. The most common detectors of the paths of particles exploit the energy lost by charged particles to ionisation.

Bubble chambers, spark chambers, and *streamer chambers* show us where particles pass through by making their tracks visible so that they may be photographed. These pictures have a high illustrative value and possess a certain aesthetic appeal. Many new particles were discovered in bubble chambers in particular in the 1950s and 1960s. These detectors are nowadays only used for special applications.

Proportional counters consist of flat, gas-filled forms in which many thin, parallel wires ($r \approx 10\,\mu\text{m}$) are arranged. The wires are maintained at a positive potential of a few kV and are typically arranged at separations of about 2 mm. Charged particles passing through the gas ionise the gas atoms in their paths and the so-released electrons drift off to the anode wires (Fig. A.7). The electric field strengths around the thin wires are very high and so the primary electrons are accelerated and reach kinetic energies such that they themselves start to ionise the gas atoms. A charge avalanche is let loose which leads to a measurable voltage pulse on the wire. The arrival time and amplitude of the pulse are registered electronically. The known position of the wire tells us where the particle passed by. The spatial resolution in the direction perpendicular to the wires is of the order of half the wire separation. An improved resolution and a reconstruction of the path in all three spatial coordinates is in practice obtained by using several layers of proportional counters with the wires pointing in different directions.

Drift chambers function similarly to proportional chambers. The wires are, however, at a few centimetres separation. The position of the particle's path x is now obtained from the time of the voltage pulse t_{wire} on the wire relative to the time t_0 that the particle crossed through the detector. This latter time has to be measured in

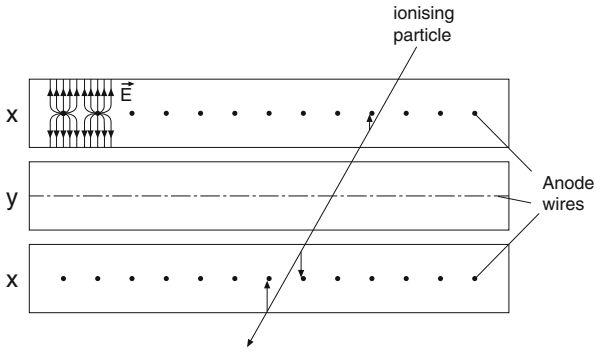

Fig. A.7 Group of three proportional chambers. The anode wires of the layers marked x point into the page, while those of the y layer run at right angles to these (*dashed line*). The cathodes are the edges of the chambers. A positive voltage applied to the anode wires generates a field like the one sketched in the *upper left hand corner*. A particle crossing through the chamber ionises the gas in its path and the electrons drift along the field lines to the anode wire. In the example shown a signal would be obtained from one wire in the upper x plane and from two in the lower x layer

another detector. Ideally we should have the linear relation

$$x = x_{\text{wire}} + v_{\text{drift}} \cdot (t_{\text{wire}} - t_0)\,, \tag{A.9}$$

if the electric field due to additional electrodes, and hence the drift velocity v_{drift} of the released electrons in the gas, are very homogeneous. Drift chambers' spatial resolution can be as good as 50 μm. Several layers are again required for a three dimensional reconstruction. Wire chambers are very useful for reconstructing paths over large areas. They may be made to cover several square metres.

Silicon strip detectors are made out of silicon crystals with very thin electrodes attached to them at separations of about, e.g., 20 μm. A charged particle crossing the wafer produces electron-hole pairs, in silicon this only requires 3.6 eV per pair. An external voltage collects the charge at the electrodes where it is registered. Spatial resolutions less than 10 μm may be reached in this way.

Measuring momenta The momenta of charged particles may be determined with the help of strong magnetic fields. The Lorentz force causes these particles to follow circular orbits which may then be, e.g., measured in bubble chamber photographs or reconstructed from several planes of wire chambers. A "rule of thumb" for the momentum component $p_\perp$ perpendicular to the magnetic field may be obtained from the measured radius of curvature of the particle path R and the known, homogeneous magnetic field B:

$$p_\perp \approx 0.3 \cdot B \cdot R \left[\frac{\text{GeV}/c}{\text{T m}}\right]. \tag{A.10}$$

Magnetic spectrometers are used to indirectly determine the radius of curvature from the angle which the particle is deflected through in the magnetic field; one measures the particle's path before and after the magnets. This method of measuring the momenta actually has smaller errors than a direct determination of the radius of curvature would have. The relative accuracy of these measurements typically decreases with increasing momenta as $\delta(p)/p \propto p$. This is because the particle path becomes straighter at high momenta.

Measuring energies A measurement of the energy of a particle usually requires the particle to be completely absorbed by some medium. The absorbed energy is transformed into ionisation, atomic excitations or perhaps Cherenkov light. This signal which may, with the help of suitable devices, be transformed into a measurable one is proportional to the original energy of the particle. The energy resolution depends upon the statistical fluctuations of the transformation process.

Semiconductor detectors are of great importance in nuclear physics. Electron-hole pairs created by charged particles are separated by an external voltage and then detected as voltage pulses. In germanium only 2.8 eV is required to produce an electron-hole pair. In silicon 3.6 eV is needed. Semiconductor detectors are typically a few millimetres thick and can absorb light nuclei with energies up to a few tens of MeV. Photon energies are determined through the photoelectric effect – one measures the signal of the absorbed photoelectron. The large number N of electron-hole pairs that are produced means that the energy resolution of such semiconductor counters is excellent, $\delta E/E \propto \sqrt{N}/N$. For 1 MeV particles it is between 10^{-3} and 10^{-4}.

Electromagnetic calorimeters may be used to measure the energies of electrons, positrons and photons above about 100 MeV. One exploits the cascade of secondary particles that these particles produce via repeated bremsstrahlung and pair production processes inside the material of the calorimeter. The production of such a measurable ionisation or visible signal is illustrated in Fig. A.8. The complete absorption of such a shower in a calorimeter takes place, depending upon the energy involved, over a distance of about 15–25 times the radiation length X_0. We will consider the example of homogeneous calorimeters made of NaI(Tl) crystals or lead glass.

NaI doped with small amounts of thallium is an inorganic scintillator in which charged particles produce visible wavelength photons. These photons may then be converted into an electric pulse with the help of photomultipliers. Calorimeters are made from large crystals of NaI(Tl) with photomultipliers attached to their backs (see Fig. 14.5). The relative energy resolution typically has values of the order of $\delta E/E \approx 1\text{–}2\,\% \,/\, \sqrt[4]{E\,[\mathrm{GeV}]}$. NaI(Tl) is also of great importance for nuclear-gamma spectroscopy, and hence for energies $\lesssim 1$ MeV, since it has a large photon absorption coefficient, particularly for the photoelectric effect.

Cascade particles in lead glass produce Cherenkov light which may also be registered with the help of photomultipliers. Lead glass calorimeters may be built up from a few thousand lead glass blocks, which can cover several square metres. The transverse dimension of these blocks is adjusted to the transverse extension of

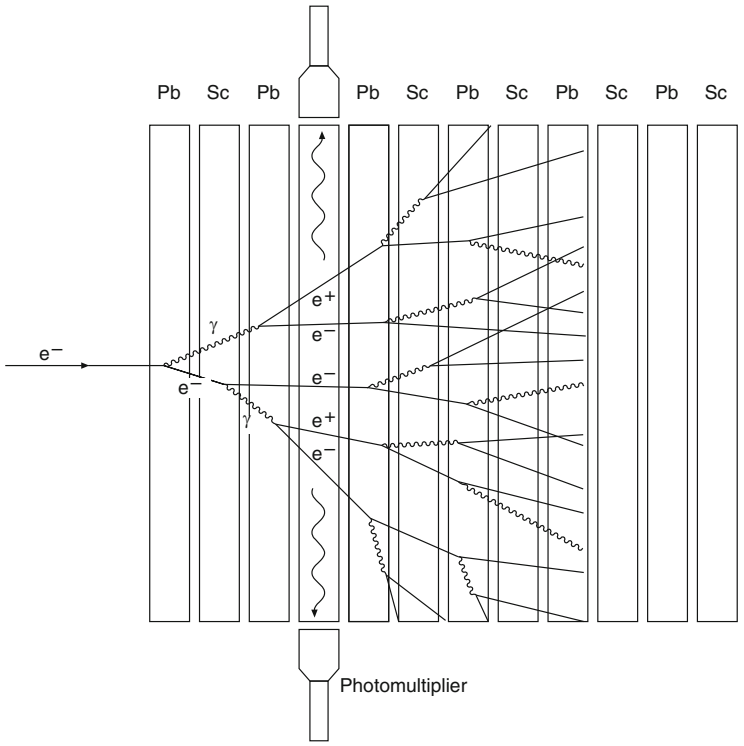

Fig. A.8 Sketch of particle cascade formation inside a calorimeter. An electromagnetic cascade inside a sampling calorimeter made out of layers of lead and scintillator is depicted. The lead acts as an absorber material where the bremsstrahlung and pair production processes primarily take place. The opening angles are, for purposes of clarity, exaggerated in the diagram. The particle tracks are for the same reason not continued on into the rearmost layers of the detector. Electrons and positrons in the scintillator produce visible scintillation light, which through total reflection inside the scintillator is led off to the sides (*large wavy lines*) where it is detected by photomultipliers. The total amount of scintillator light measured is proportional to the energy of the incoming electron

electromagnetic showers, typically a few centimetres. Energy resolution is typically around $\delta E/E \approx 3-5\,\% \,/\, \sqrt{E\,[\mathrm{GeV}]}$.

Hadronic calorimeters may be used to measure hadronic energies. These produce a shower of secondary particles (mostly further hadrons) in inelastic reactions. Such hadronic showers have, compared to electromagnetic showers, a larger spatial extension and display much larger fluctuations in both the number and type of secondary particles involved. *Sampling calorimeters* made up of alternating layers of a pure absorber material (e.g., iron, uranium) and a detector material (e.g., an organic scintillator) are used to measure hadron energies. Only a small fraction of the original particle's energy is deposited in the detector material. The energy resolution of hadronic calorimeters is, both for this reason and because of the

large fluctuations in the number of secondary particles, only about $\delta E/E \approx 30-80\,\%/\sqrt{E\,[\mathrm{GeV}]}$.

Momentum and energy measurements are interchangeable for highly relativistic particles (5.6). The accuracy of momentum measurements in magnetic spectrometers decreases linearly with particle momentum, while the precision of energy measurements in calorimeters increases as $1/\sqrt{E}$. Depending upon the particle type and the particular detector configuration it can make sense for particles with momenta above 50–100 GeV to measure momenta indirectly through a more accurate energy measurement in a calorimeter.

Identifying particles The mass and the charge of a particle generally suffice to identify it. The sign of a particle's charge may be easily read off from the particle's deflection in a magnetic field, but a direct measurement of the particle's mass is mostly impossible. There is therefore no general particle identification recipe; rather lots of different methods, which often use other particle properties, are available. Subsequently, we will briefly list those methods which are used in particle physics for particles with momenta above about 100 MeV/c.

- Short lived particles may be identified from their decay products with the help of the method of invariant masses (cf. Sect. 16.1).
- The presence of neutrinos is usually only detected by measuring a deficit of energy or momentum in a reaction.
- Electrons and photons are recognised through their characteristic electromagnetic showers in calorimeters. We may distinguish between them by putting an ionisation detector (e.g., a scintillator or a wire chamber) in front of the calorimeter – of the two only an electron will leave an ionisation trail.
- Muons are identified by their exceptional penetrative powers. They primarily lose energy to ionisation and may be detected with the help of ionisation chambers placed behind lead plates, which will absorb all other charged particles.
- Charged hadrons, such as pions, kaons and protons, are the most difficult particles to distinguish. For them not only a momentum measurement is required but also a further independent measurement is needed – which one is best suited depends upon the particle's momentum.
  - The time of flight between two ionisation detectors may be measured for momenta below 1 GeV/c, since the velocity depends for a fixed momentum upon the mass. A further possibility is to measure the loss of energy to ionisation – this depends upon the particle velocity. In this range it varies as $1/v^2$.
  - This latter approach may be extended to 1.5–50 GeV/c momenta (where the energy loss only increases logarithmically as $\beta = v/c$) if the measurements are performed repeatedly.

- Various sorts of *Cherenkov counters* may be used in the range up to about 100 GeV/c. Threshold Cherenkov counters require a material with a refractive index n so arranged that only specific particles with a particular momentum can produce Cherenkov light (cf. A.8). In ring imaging Cherenkov counters (RICH) the opening angle of the Cherenkov photons is measured for all the particles and their speed may be calculated from this. If their momentum is known then this determines their identity.
- *Transition radiation detectors* may be used for $\gamma = E/mc^2 \gtrsim 100$. Transition radiation is produced when charged particles cross from one material to another which has a different dielectric constant. The intensity of the radiation depends upon γ. Thus an intensity measurement can enable us to distinguish between different hadrons with the same momenta. This is in fact the only way to identify such particles if the energy of the hadron is above 100 GeV. Transition radiation may also be employed to distinguish between electrons and pions. The tiny mass of the electrons means that this is already possible for energies around 1 GeV.

– Neutron detection is a special case; (n, α) and (n, p) nuclear reactions are used to identify neutrons – from those with thermal energies to those with momenta up to around 20 MeV/c. The charged reaction products have fixed kinetic energies and these may be measured in scintillation counters or gas ionisation counters. For momenta between 20 MeV/c and 1 GeV/c one looks for protons from elastic neutron-proton scattering. The proton target is generally part of the material of the detector itself (plastic scintillator, counter gas). At higher momenta only hadron calorimeter measurements are available to us. The identification is then, however, as a rule not unambiguous.

A detector system We wish to present as an example of a system of detectors the ZEUS detector at the HERA storage ring. This detector measured the reaction products in high energy electron-proton collisions with centre-of-mass energies up to about 320 GeV (Fig. A.9). It was so arranged that apart from the beam pipe region the reaction zone was hermetically covered. Many different detectors, chosen to optimise the measurement of energy and momentum and the identification of the reaction products, made up the whole. The most important components are the wire chambers, which were arranged directly around the reaction point, and, just outside these, a uranium-scintillator calorimeter where the energies of electrons and hadrons were measured to a high precision.

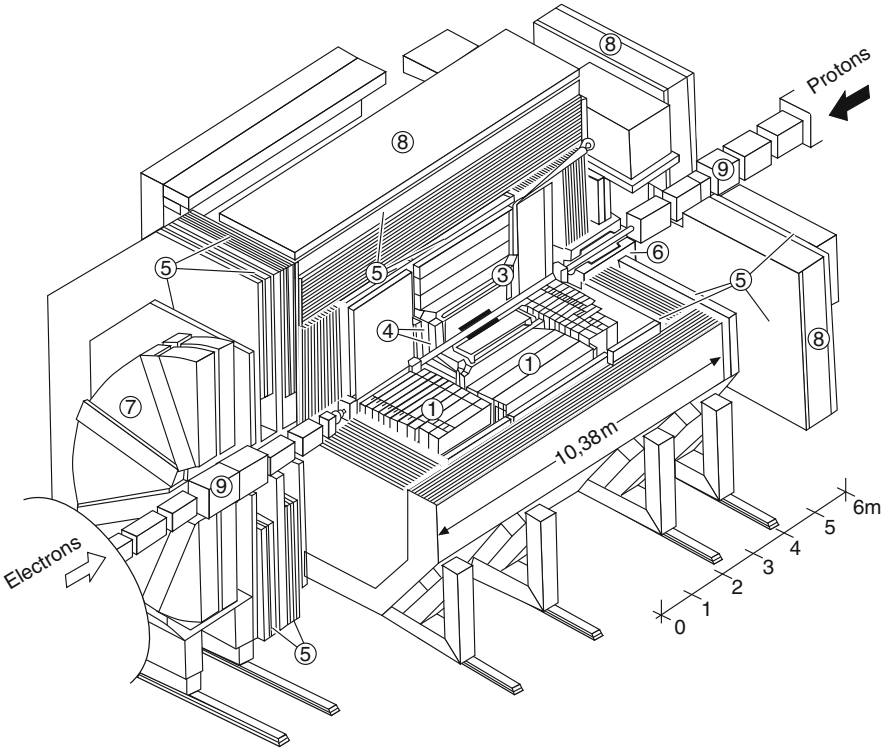

Fig. A.9 The ZEUS detector at the HERA storage ring in DESY. The electrons and protons are focused with the help of magnetic lenses (*9*) before they are made to collide at the interaction point in the centre of the detector. The tracks of charged reaction products are registered in the vertex chamber (*3*) which surrounds the reaction point and also in the central track chamber (*4*). These drift chambers are surrounded by a superconducting coil which produces a magnetic field of up to 1.8 T. The influence of this magnetic field on the electron beam which passes through it must be compensated by additional magnets (*6*). The next layer is a uranium-scintillator calorimeter (*1*) where the energies of electrons, photons and also of hadrons may be measured to a great accuracy. The iron yoke of the detector (*2*), into which the magnetic flux of the central solenoid returns, also acts as an absorber for the backwards calorimeter, where the energy of those high energy particle showers that are not fully absorbed in the central uranium calorimeter may be measured. Large area wire chambers (*5*), positioned behind the iron yoke, surround the whole detector and are used to betray the passage of any muons. These chambers may be used to measure the muons' momenta since they are inside either the magnetic field of the iron yoke or an additional 1.7 T toroidal field (*7*). Finally a thick reinforced concrete wall (*8*) screens off the experimental hall as far as is possible from the radiation produced in the reactions (*Courtesy of DESY*)

A.3 Combining Angular Momenta

The combination of two angular momenta $|j_1 m_1\rangle$ and $|j_2 m_2\rangle$ to form a total angular momentum $|JM\rangle$ must obey the following selection rules:

$$|j_1 - j_2| \leq J \leq j_1 + j_2 \,, \tag{A.11}$$

$$M = m_1 + m_2 \,, \tag{A.12}$$

$$J \geq |M| \,. \tag{A.13}$$

The coupled states may be expanded with the help of the *Clebsch-Gordan coefficients* (CGC) $(j_1 j_2 m_1 m_2 | JM)$ in the $|j_1\ j_2\ JM\rangle$ basis:

$$|j_1\, m_1\rangle \otimes |j_2\, m_2\rangle \;=\; \sum_{\substack{J=|j_1-j_2| \\ M=m_1+m_2}}^{J=j_1+j_2} (j_1\ j_2\, m_1\, m_2|JM) \cdot |j_1\ j_2\, JM\rangle \,. \tag{A.14}$$

The probability that the combination of two angular momenta $|j_1 m_1\rangle$ and $|j_2 m_2\rangle$ produces a system with total angular momentum $|JM\rangle$ is thus the square of the corresponding CGC's.

The corollary

$$|j_1\ j_2\, JM\rangle \;=\; \sum_{\substack{m_1=-j_1 \\ m_2=M-m_1}}^{m_1=+j_1} (j_1\ j_2\, m_1\, m_2|JM) \cdot |j_1\, m_1\rangle \otimes |j_2\, m_2\rangle \,, \tag{A.15}$$

also holds. For a system $|JM\rangle$, which has been produced from a combination of two angular momenta j_1 and j_2, the square of the CGC's gives the probability that the individual angular momenta may be found in the states $|j_1 m_1\rangle$ and $|j_2 m_2\rangle$.

Equations (A.14) and (A.15) may also be applied to isospin. Consider, for example, the Δ^+ baryon ($I = 3/2, I_3 = +1/2$) which can decay into $\mathrm{p} + \pi^0$ or $\mathrm{n} + \pi^+$. The branching ratio can be found to be

$$\frac{B(\Delta^+ \to \mathrm{p} + \pi^0)}{B(\Delta^+ \to \mathrm{n} + \pi^+)} \;=\; \frac{\left|\left(\tfrac{1}{2}\ 1\ +\tfrac{1}{2}\ \ 0\ \middle|\ \tfrac{3}{2}\ +\tfrac{1}{2}\right)\right|^2}{\left|\left(\tfrac{1}{2}\ 1\ -\tfrac{1}{2}\ +1\ \middle|\ \tfrac{3}{2}\ +\tfrac{1}{2}\right)\right|^2} \;=\; \frac{\left(\sqrt{\tfrac{2}{3}}\right)^2}{\left(\sqrt{\tfrac{1}{3}}\right)^2} \;=\; 2 \,. \tag{A.16}$$

The CGC's are listed for combinations of low angular momenta. The values for $j_1 = 1/2$ and $j_2 = 1$ may be found with the help of the general phase relation

$$(j_2\ j_1\, m_2\, m_1|JM) = (-1)^{j_1+j_2-J} \cdot (j_1\ j_2\, m_1\, m_2|JM) \,. \tag{A.17}$$

$j_1 = 1/2$		$j_2 = 1/2$		
m_1	m_2	J	M	CGC
$1/2$	$1/2$	1	1	$+1$
$1/2$	$-1/2$	1	0	$+\sqrt{1/2}$
$1/2$	$-1/2$	0	0	$+\sqrt{1/2}$
$-1/2$	$1/2$	1	0	$+\sqrt{1/2}$
$-1/2$	$1/2$	0	0	$-\sqrt{1/2}$
$-1/2$	$-1/2$	1	-1	$+1$

$j_1 = 1$		$j_2 = 1/2$		
m_1	m_2	J	M	CGC
1	$1/2$	$3/2$	$3/2$	$+1$
1	$-1/2$	$3/2$	$1/2$	$+\sqrt{1/3}$
1	$-1/2$	$1/2$	$1/2$	$+\sqrt{2/3}$
0	$1/2$	$3/2$	$1/2$	$+\sqrt{2/3}$
0	$1/2$	$1/2$	$1/2$	$-\sqrt{1/3}$
0	$-1/2$	$3/2$	$-1/2$	$+\sqrt{2/3}$
0	$-1/2$	$1/2$	$-1/2$	$+\sqrt{1/3}$
-1	$1/2$	$3/2$	$-1/2$	$+\sqrt{1/3}$
-1	$1/2$	$1/2$	$-1/2$	$-\sqrt{2/3}$
-1	$-1/2$	$3/2$	$-3/2$	$+1$

$j_1 = 1$		$j_2 = 1$		
m_1	m_2	J	M	CGC
1	1	2	2	$+1$
1	0	2	1	$+\sqrt{1/2}$
1	0	1	1	$+\sqrt{1/2}$
1	-1	2	0	$+\sqrt{1/6}$
1	-1	1	0	$+\sqrt{1/2}$
1	-1	0	0	$+\sqrt{1/3}$
0	1	2	1	$+\sqrt{1/2}$
0	1	1	1	$-\sqrt{1/2}$
0	0	2	0	$+\sqrt{2/3}$
0	0	1	0	0
0	0	0	0	$-\sqrt{1/3}$
0	-1	2	-1	$+\sqrt{1/2}$
0	-1	1	-1	$+\sqrt{1/2}$
-1	1	2	0	$+\sqrt{1/6}$
-1	1	1	0	$-\sqrt{1/2}$
-1	1	0	0	$-\sqrt{1/3}$
-1	0	2	-1	$+\sqrt{1/2}$
-1	0	1	-1	$-\sqrt{1/2}$
-1	-1	2	-2	$+1$

A.4 Physical Constants

Table A.1 Physical constants [3, 8, 12]. The numbers in brackets signify the uncertainty in the last decimal places. The sizes of c, μ_0 (and hence ε_0) are defined by the units "metre" and "ampere" [13]. These constants are therefore error free

Constants	Symbol	Value
Speed of light	c	$2.997\,924\,58 \cdot 10^8$ m s^{-1}
Planck's constant	h	$6.626\,069\,57\,(29) \cdot 10^{-34}$ J s
	$\hbar = h/2\pi$	$1.054\,571\,726\,(47) \cdot 10^{-34}$ J s
		$= 6.582\,119\,28\,(15) \cdot 10^{-22}$ MeV s
	$\hbar c$	197.326 9718 (44) MeV fm
	$(\hbar c)^2$	0.389 379 338 (17) GeV^2 mbarn
Atomic mass unit	$u = M_{^{12}\mathrm{C}}/12$	931.494 061 (21) MeV/c^2
Mass of the proton	M_p	938.272 046 (21) MeV/c^2

(continued)

Table A.1 (continued)

Constants	Symbol	Value
Mass of the neutron	M_n	939.565 379 (21) MeV/c^2
Mass of the electron	m_e	0.510 998 928 (11) MeV/c^2
Elementary charge	e	$1.602\,176\,565\,(35) \cdot 10^{-19}$ A s
Dielectric constant	$\varepsilon_0 = 1/\mu_0 c^2$	$8.854\,187\,817 \cdot 10^{-12}$ A s/V m
Permeability of vacuum	μ_0	$4\pi \cdot 10^{-7}$ V s/A m
Fine structure constant	$\alpha = e^2/4\pi\varepsilon_0\hbar c$	1/137.035 999 074 (44)
Class. electron radius	$r_e = \alpha\hbar c/m_e c^2$	$2.817\,940\,3267\,(27) \cdot 10^{-15}$ m
Compton wavelength	$\lambda\!\!\!^{-}_e = r_e/\alpha$	$3.861\,592\,6800\,(25) \cdot 10^{-13}$ m
Bohr radius	$a_0 = r_e/\alpha^2$	$5.291\,772\,1092\,(17) \cdot 10^{-11}$ m
Bohr magneton	$\mu_B = e\hbar/2m_e$	$5.788\,381\,8066\,(38) \cdot 10^{-11}$ MeV T^{-1}
Nuclear magneton	$\mu_N = e\hbar/2m_p$	$3.152\,451\,2605\,(22) \cdot 10^{-14}$ MeV T^{-1}
Magnetic moment	μ_e	1.001 159 652 180 76 (27) μ_B
	μ_p	2.792 847 356 (23) μ_N
	μ_n	−1.913 042 72 (45) μ_N
Avogadro's number	N_A	$6.022\,141\,29\,(27) \cdot 10^{23}$ mol^{-1}
Boltzmann's constant	k	$1.380\,6488\,(13) \cdot 10^{-23}$ J K^{-1}
		$= 8.617\,3324\,(78) \cdot 10^{-5}$ eV K^{-1}
Gravitational constant	G	$6.673\,84\,(80) \cdot 10^{-11}$ N m^2 kg^{-2}
	$G/\hbar c$	$6.708\,37\,(80) \cdot 10^{-39}$ (GeV/c^2)$^{-2}$
Fermi constant	$G_F/(\hbar c)^3$	$1.166\,378\,7\,(6) \cdot 10^{-5}$ GeV^{-2}
Weinberg angle	$\sin^2\theta_W$	0.231 16 (12)
Mass of the $W^{\pm}$	M_W	80.385 (15) GeV/c^2
Mass of the Z^0	M_Z	91.1876 (21) GeV/c^2
Strong coupling const.	$\alpha_s(M_Z^2 c^2)$	0.1184 (7)

Solutions to Problems

Chapter 2

1. Proton repulsion in ^{3}He:

$$\begin{aligned} V_{\mathrm{C}} &= \tfrac{-\hbar c\alpha}{R} = (M_{^3\mathrm{He}} - M_{^3\mathrm{H}}) \cdot c^2 - \left(M_{\mathrm{n}} - M_{\mathrm{p}}\right) \cdot c^2 \\ &= E_{\beta}^{\max} - \left(M_{\mathrm{n}} - M_{\mathrm{p}} - m_{\mathrm{e}}\right) \cdot c^2 \,. \end{aligned}$$

This yields $R = 1.88\,\mathrm{fm}$. The β-decay recoil and the difference between the atomic binding energies may be neglected.

Chapter 3

1. (a) At Saturn we have $t/\tau = 4\,\mathrm{years}/127\,\mathrm{years}$ and we require

$$N_0 \frac{1}{\tau} \mathrm{e}^{-t/\tau} \cdot 5.49\,\mathrm{MeV} \cdot 0.055 = 395\,\mathrm{W}$$

power to be available. This implies $N_0 = 3.4 \cdot 10^{25}$ nuclei, which means $13.4\,\mathrm{kg}$ ^{238}Pu.

(b) At Neptune (after 12 years) 371 W would be available.

(c) The power available from radiation decreases as $1/r^2$. Hence at Saturn 395 W power would require an area of $2.5 \cdot 10^3\,\mathrm{m}^2$ and 371 W at Neptune could be produced by an area of $2.3 \cdot 10^4\,\mathrm{m}^2$. This would presumably lead to construction and weight problems.

B. Povh et al., *Particles and Nuclei*, Graduate Texts in Physics,
DOI 10.1007/978-3-662-46321-5

2. (a) Applying the formula $N = N_0 \mathrm{e}^{-\lambda t}$ to both uranium isotopes leads to

$$\frac{99.28}{0.72} = \frac{\mathrm{e}^{-\lambda_{238} t}}{\mathrm{e}^{-\lambda_{235} t}} \quad \text{which yields:} \quad t = 5.9 \cdot 10^9 \text{ years.}$$

Uranium isotopes, like all heavy ($A \gtrsim 56$) elements, are produced in supernova explosions. The material which is so ejected is used to build up new stars. The isotopic analysis of meteorites leads to the age of the solar system being $4.55 \cdot 10^9$ years.

(b) After $2.5 \cdot 10^9$ years, $(1 - \mathrm{e}^{-\lambda t})$ of the nuclei will have decayed. This is 32 %.

(c) Equation (2.8) yields that a total of 51 MeV is released in the $^{238}\mathrm{U} \rightarrow {}^{206}\mathrm{Pb}$ decay chain. In spontaneous fission 190 MeV is set free.

3. (a)

$$A_2(t) = N_{0,1} \cdot \lambda_1 \cdot \frac{\lambda_2}{\lambda_2 - \lambda_1} \left(\mathrm{e}^{-\lambda_1 t} - \mathrm{e}^{-\lambda_2 t} \right)$$

for large times t, because of $\lambda_1 \ll \lambda_2$:

$$A_2(t) = N_{0,1} \cdot \lambda_1 .$$

(b) The concentration of $^{238}\mathrm{U}$ in concrete can thus be found to be

$$\begin{array}{ll} \text{room volume} & V\text{: } 400 \text{ m}^3 \\ \text{eff. concrete volume} & V_\mathrm{B}\text{: } 5.4 \text{ m}^3 \end{array} \implies \varrho_\mathrm{U} = \frac{V \cdot A}{V_\mathrm{B} \cdot \lambda_{238}} = 1.5 \cdot 10^{21} \, \frac{\text{atoms}}{\text{m}^3} .$$

4. Nuclear masses for fixed A depend quadratically upon Z. From the definitions in (3.6) the minimum of the parabola is at $Z_0 = \beta / 2\gamma$. The constant a_a in β and γ is part of the asymmetry term in the mass formula (2.8) and, according to (18.12), does not depend upon the electromagnetic coupling constant α. The "constant" a_c, which describes the Coulomb repulsion and enters the definition of γ, is on the other hand proportional to α and may be written as: $a_\mathrm{c} = \kappa\alpha$. Inserting this into $Z_0 = \beta / 2\gamma$ yields

$$Z_0 = \frac{\beta}{2\left(a_\mathrm{a}/A + \kappa\alpha/A^{1/3}\right)} \qquad \Longrightarrow \qquad \frac{1}{\alpha} = \frac{2\kappa A Z_0}{A^{1/3}\left(A\beta - 2a_\mathrm{a} Z_0\right)} .$$

Assuming that the minimum of the mass formula is exactly at the given Z one finds $1/\alpha$ values of 128, 238 and 522 for the ${}^{186}_{74}\mathrm{W}$, ${}^{186}_{82}\mathrm{Pb}$ and ${}^{186}_{88}\mathrm{Ra}$ nuclides. Stable ${}^{186}_{94}\mathrm{Pu}$ cannot be obtained just by "twiddling" α.

5. The energy E released in ${}^{A}_{Z}\mathrm{X} \rightarrow {}^{A-4}_{Z-2}\mathrm{Y} + \alpha$ is

$$E = B(\alpha) - \delta B \qquad \text{where} \quad \delta B = B(\mathrm{X}) - B(\mathrm{Y}) .$$

Note that we have here neglected the difference in the atomic binding energies. If we further ignore the pairing energy, which only slightly changes, we obtain

$$E = B(\alpha) - \frac{\partial B}{\partial Z}\delta Z - \frac{\partial B}{\partial A}\delta A \;=\; B(\alpha) - 2\frac{\partial B}{\partial Z} - 4\frac{\partial B}{\partial A}$$
$$= B(\alpha) - 4a_\mathrm{v} + \frac{8}{3}a_\mathrm{s}\frac{1}{3A^{1/3}} + 4a_\mathrm{c}\frac{Z}{A^{1/3}}\left(1 - \frac{Z}{3A}\right) - a_\mathrm{a}\left(1 - \frac{2Z}{A}\right)^2 .$$

Putting in the parameters yields $E > 0$ if $A \gtrsim 150$. Natural α-activity is only significant for $A \gtrsim 200$, since the lifetime is extremely long for smaller mass numbers.

6. The mother nucleus and the α particle are both 0^+ systems which implies that the spin J and parity P of a daughter nucleus with orbital angular momentum L and spatial wave function parity $(-1)^L$ must combine to 0^+. This means that $J^P = 0^+, 1^-, 2^+, 3^-, \ldots$ are allowed.

Chapter 4

1. (a) In analogy to (4.5) the reaction rate must obey $\dot{N} = \sigma \dot{N}_\mathrm{d} n_\mathrm{t}$, where $\dot{N}_\mathrm{d}$ signifies the deuteron particle current and n_t is the particle areal density of the tritium target. The neutron rate found in any solid angle element $\mathrm{d}\Omega$ must then obey

$$\mathrm{d}\dot{N} = \frac{\mathrm{d}\sigma}{\mathrm{d}\Omega}\,\mathrm{d}\Omega\,\dot{N}_\mathrm{d}\,n_\mathrm{t} = \frac{\mathrm{d}\sigma}{\mathrm{d}\Omega}\,\frac{F}{R^2}\,\frac{I_\mathrm{d}}{e}\,\frac{\mu_\mathrm{t}}{m_\mathrm{t}}\,N_\mathrm{A}\,,$$

where e is the elementary electric charge, m_t is the molar mass of tritium and N_A is Avogadro's number.
Inserting the numbers yields $\mathrm{d}\dot{N} = 1{,}444$ neutrons/s.

(b) Rotating the target away from the orthogonal increases the effective particle area density "seen" by the beam by a factor of $1/\cos\theta$. A rotation through $10°$ thus increases the reaction rate by 1.5 %.

2. The number N of beam particles decreases according to (4.5) with the distance x covered as $\mathrm{e}^{-x/\lambda}$ where $\lambda = 1/\sigma n$ is the absorption length.

(a) Thermal neutrons in cadmium: We have

$$n_\mathrm{Cd} = \varrho_\mathrm{Cd}\frac{N_\mathrm{A}}{A_\mathrm{Cd}}\,,$$

where the atomic mass of cadmium is given by $A_\mathrm{Cd} = 112.40\,\mathrm{g\,mol^{-1}}$. We thus obtain

$$\lambda_\mathrm{n,Cd} = 9\,\mu\mathrm{m}\,.$$

(b) For highly energetic photons in lead one may find in an analogous manner ($A_{\mathrm{Pb}} = 207.19\,\mathrm{g\,mol^{-1}}$)

$$\lambda_{\gamma,\mathrm{Pb}} = 2.0\,\mathrm{cm}\,.$$

(c) Antineutrinos predominantly react with the electrons in the Earth. Their density is

$$n_{\mathrm{e,Earth}} = \varrho_{\mathrm{Earth}} \left(\frac{Z}{A}\right)_{\mathrm{Earth}} N_{\mathrm{A}}.$$

We therefore obtain

$$\lambda_{\overline{\nu}/\mathrm{Earth}} = 6.7 \cdot 10^{16}\,\mathrm{m}\,,$$

which is about $5 \cdot 10^9$ times the diameter of the planet.

Note: the number of beam particles only decreases exponentially with distance if *one* reaction leads to the beam particles being absorbed; a criterion which is fulfilled in the above examples. The situation is different if $k \gg 1$ reactions are needed (e.g., α particles in air). In such cases the range is almost constant $L = k/\sigma n$.

Chapter 5

1. (a) From $Q^2 = -(p - p')^2$ and (5.13) one finds

$$Q^2 = 2M(E - E')\,,$$

with M the mass of the heavy nucleus. This implies that Q^2 is largest at the smallest value of E', i.e., $\theta = 180°$. The maximal momentum transfer is then from (5.15)

$$Q^2_{\mathrm{max}} = \frac{4E^2M}{Mc^2 + 2E}\,,$$

(b) From (5.15) we find for $\theta = 180°$ that the energy transfer $\nu = E - E'$ is

$$\nu = E\left(1 - \frac{1}{1 + 2\frac{E}{Mc^2}}\right) = \frac{2E^2}{Mc^2 + 2E}\,.$$

The energy of the backwardly scattered nucleus is then

$$E'_{\text{nucleus}} = Mc^2 + \nu = Mc^2 + \frac{2E^2}{Mc^2 + 2E}$$

and its momentum is

$$|\boldsymbol{P}'| = \sqrt{Q_{\max}^2 + \frac{\nu^2}{c^2}} = \sqrt{\frac{4ME^2}{Mc^2 + 2E} + \frac{4E^4}{c^2(Mc^2 + 2E)^2}} \,.$$

(c) The nuclear Compton effect may be calculated with the help of $\Delta\lambda = \frac{h}{Mc}(1 - \cos\theta)$. The same result as for electron scattering is obtained since we have neglected the electron rest mass in (a) and (b) above.

2. Those α particles which directly impinge upon the ^{56}Fe nucleus are absorbed. Elastically scattered α particles correspond to a "shadow scattering" which may be described as Fraunhofer diffraction upon a disc. The diameter D of the disc is found to be

$$D = 2(\sqrt[3]{4} + \sqrt[3]{56}) \cdot 0.94 \text{ fm} \approx 10 \text{ fm} \,.$$

In the literature D is mostly parametrised by the formula $D = 2\sqrt[3]{A} \cdot 1.3\text{fm}$, which gives the same result. The wavelength of the α particles is $\lambda = h/p$, where p is to be understood as that in the centre-of-mass system of the reaction. Using $pc = 840$ MeV one finds $\lambda = 1.5$ fm.
The first minimum is at $\theta = 1.22\,\lambda/D \approx 0.18 \approx 10.2°$. The intensity distribution of the diffraction is given by the Bessel function j_0. The further minima correspond to the nodes of this Bessel function.
The scattering angle ought, however, to be given in the laboratory frame and is given by $\theta_{\text{lab}} \approx 9.6°$.

3. The smallest separation of the α particles from the nucleus is $s(\theta) = a + \frac{a}{\sin\theta/2}$ for the scattering angle θ. The parameter a is obtained from 180° scattering, since the kinetic energy is then equal to the potential energy:

$$E_{\text{kin}} = \left| \frac{zZe^2\hbar c}{4\pi\varepsilon_0 \hbar c 2a} \right| .$$

For 6 MeV α scattering off gold, we have $a = 19\,\text{fm}$ and $s = 38\,\text{fm}$. For deviations from Rutherford scattering to occur, the α particles must manage to get close to the nuclear forces, which can first happen at a separation $R = R_\alpha + R_{\text{Au}} \approx 9$ fm. A more detailed discussion is given in Sect. 19.4. Since $s \gg R$ no nuclear reactions are possible between 6 MeV α particles and gold and no deviation from the Rutherford cross-section should therefore be expected. This would only be possible for much lighter nuclei.

4. The kinetic energy of the electrons may be found as follows:

$$\frac{\hbar}{\sqrt{2M_\alpha E_\alpha^{\rm kin}}} \approx \lambda\!\!\!^{-}_\alpha \stackrel{!}{=} \lambda\!\!\!^{-}_{\rm e} \approx \frac{\hbar c}{E_{\rm e}^{\rm kin}} \Longrightarrow E_{\rm e}^{\rm kin} \approx \sqrt{2M_\alpha c^2 E_\alpha^{\rm kin}} = 211\,{\rm MeV}\,.$$

The momentum transfer is maximal for scattering through 180°. Neglecting the recoil we have

$$|\boldsymbol{q}|_{\rm max} = 2|\boldsymbol{p}_{\rm e}| = \frac{2\hbar}{\lambda\!\!\!^{-}_{\rm e}} \approx 2\sqrt{2M_\alpha E_\alpha^{\rm kin}} = 423\,{\rm MeV}/c\,,$$

and the variable α in Table 5.1 may be found with the help of (5.56) to be

$$\alpha_{\rm max} = \frac{|\boldsymbol{q}|_{\rm max} R}{\hbar} = \frac{423\,{\rm MeV}\cdot 1.21\cdot \sqrt[3]{197}\,{\rm fm}}{197\,{\rm MeV\,fm}} = 15.1\,.$$

The behaviour of the function $3\,\alpha^{-3}\,(\sin\alpha - \alpha\cos\alpha)$ from Table 5.1 is such that it has 4 zero points in the range $0 < \alpha \leq 15.1$.

5. Electrons oscillate most in the field of the X-rays since $M_{\rm nuclear} \gg m_{\rm e}$. As in the H atom, the radial wave function of the electrons also falls off exponentially in He. Hence, just as for electromagnetic electron scattering off nucleons, a dipole form factor is observed.
6. If a 511 keV photon is Compton scattered through 30° off an electron at rest, the electron receives momentum, $p_{\rm e} = 0.26\,{\rm MeV}/c$. From the virial theorem an electron bound in a helium atom must have kinetic energy $E_{\rm kin} = -E_{\rm pot}/2 = -E_{\rm tot} = 24$ eV, which implies that the momentum of the Compton electron is smeared out with $\Delta p \approx \pm 5\cdot 10^{-3}$ MeV/c which corresponds to an angular smearing of $\Delta\theta_{\rm e} \approx \Delta p/p = \pm 20$ mrad $\approx \pm 1°$.

Chapter 6

1. The form factor of the electron must be measured up to $|\boldsymbol{q}| \approx \hbar/r_0 = 200\,{\rm GeV}/c$. One thus needs $\sqrt{s} = 200$ GeV, i.e., 100 GeV colliding beams. For a target at rest, $2m_{\rm e}c^2E = s$ implies that $4\cdot 10^7$ GeV (!) would be needed.
2. Since the pion has spin zero, the magnetic form factor vanishes and we have (6.10):

$$\frac{{\rm d}\sigma({\rm e}\pi \to {\rm e}\pi)}{{\rm d}\Omega} = \left(\frac{{\rm d}\sigma}{{\rm d}\Omega}\right)_{\rm Mott} G_{E,\pi}^2(Q^2)$$

$$G_{E,\pi}^2(Q^2) \approx \left(1 - \frac{Q^2\,\langle r^2\rangle_\pi}{6\,\hbar^2}\right)^2 = 1 - 3.7\,\frac{Q^2}{{\rm GeV}^2/c^2}\,.$$

Chapter 7

1. Comparing the coefficients in (6.5) and (7.8) yields

$$\frac{2W_1}{W_2} = 2\tau\,, \qquad \text{where} \qquad \tau = \frac{Q^2}{4m^2c^2}\,,$$

and m is the mass of the target. Replacing W_1 by F_1/Mc^2 and W_2 by F_2/ν means that we can write

$$\frac{\nu}{Mc^2} \cdot \frac{F_1}{F_2} = \frac{Q^2}{4m^2c^2}\,.$$

Since we consider elastic scattering off a particle with mass m we have $Q^2 = 2m\nu$ and thus

$$m = \frac{Q^2}{2\nu} = x \cdot M \qquad \text{since} \quad x = \frac{Q^2}{2M\nu}\,.$$

Inserting this mass into the above equation yields (7.11).

2. The squared four momentum of the scattered parton is $(q + \xi P)^2 = m^2c^2$, where m is the mass of the parton. Expanding and multiplying with x^2/Q^2 yields

$$\frac{x^2M^2c^2}{Q^2}\xi^2 + x\xi - x^2\left(1 + \frac{m^2c^2}{Q^2}\right) = 0\,.$$

Solving the quadratic equation for ξ and employing the approximate formula given in the question yields the result we were asked to obtain. For $m = xM$ we have $x = \xi$. In a rapidly moving frame of reference we also have $x = \xi$, since the masses m and M can then be neglected.

Chapter 8

1. (a) From $x = Q^2/2M\nu$ we obtain $x \gtrsim 0.003$.
   (b) The average number of resolved partons is given by the integral over the parton distributions from $x_{\min}$ to 1. The normalisation constant, A, has to be chosen such that the number of valence quarks is exactly 3. One finds:

	Sea quarks	Gluons
$x > 0.3$	0.005	0.12
$x > 0.03$	0.4	4.9

2. (a) The centre-of-mass energy of the electron-proton collision calculated from

$$s = (p_\mathrm{p}c + pc)^2 = M^2c^4 + m^2c^4 + 2(E_\mathrm{p}E - \boldsymbol{p}_\mathrm{p} \cdot \boldsymbol{p}c^2) \approx 4E_\mathrm{p}E$$

is

$$\sqrt{s} = 319\,\mathrm{GeV}\,,$$

if we neglect the electron and proton masses. For a stationary proton target ($E_\mathrm{p} = Mc^2$; $\boldsymbol{p}_\mathrm{p} = \boldsymbol{0}$) the squared centre-of-mass energy of the electron-proton collision is found to be $s \approx 2EMc^2$. The electron beam energy would have to be

$$E = \frac{s}{2Mc^2} = 54.1\,\mathrm{TeV}$$

to attain a centre-of-mass energy $\sqrt{s} = 319\,\mathrm{GeV}$.

(b) Consider the underlying electron-quark scattering reaction $\mathrm{e}(E) + \mathrm{q}(xE_\mathrm{p}) \rightarrow \mathrm{e}(E') + \mathrm{q}(E'_\mathrm{q})$, where the bracketed quantities are the particle energies. Energy and momentum conservation yield the following three relations:

(1) $E + xE_\mathrm{p} = E' + E'_\mathrm{q}$	overall energy
(2) $E' \sin\theta/c = E'_\mathrm{q} \sin\gamma/c$	transverse momentum
(3) $(xE_\mathrm{p} - E)/c = (E'_\mathrm{q} \cos\gamma - E' \cos\theta)/c$	longitudinal momentum.

Q^2 may be expressed in terms of the electron parameters E, E' and θ as (6.2)

$$Q^2 = 2EE'(1 - \cos\theta)/c^2\,.$$

We now want to replace E' with the help of (1)-(3) by E, θ and γ. After some work we obtain

$$E' = \frac{2E \sin\gamma}{\sin\theta + \sin\gamma - \sin(\theta - \gamma)}$$

and thus

$$Q^2 = \frac{4E^2 \sin\gamma(1 - \cos\gamma)}{[\sin\theta + \sin\gamma - \sin(\theta - \gamma)]\,c^2}\,.$$

Experimentally the scattering angle γ of the scattered quark may be expressed in terms of the energy-weighted average angle of the hadronisation products

$$\cos\gamma = \frac{\sum_i E_i \cos\gamma_i}{\sum_i E_i}\,.$$

(c) The greatest possible value of Q^2 is $Q^2_{\max} = s/c^2$. This occurs for electrons scattering through $\theta = 180°$ (backward scattering) when the energy is completely transferred from the proton to the electron, $E' = E_p$. At HERA $Q^2_{\max} = 10^5\ (\mathrm{GeV}/c)^2$, while for experiments with a static target and beam energy $E = 300\,\mathrm{GeV}$ we have $Q^2_{\max} = 2EM \approx 560\ (\mathrm{GeV}/c)^2$. The spatial resolution is $\Delta x \simeq \hbar/Q$ which for the cases at hand is $0.62 \cdot 10^{-3}$ fm and $8.3 \cdot 10^{-3}$ fm respectively, i.e., a thousandth or a hundredth of the proton radius. In practice the fact that the cross-section falls off very rapidly at large Q^2 means that measurements are only possible up to about $Q^2_{\max}/2$.

(d) The minimal value of Q^2 is obtained at the minimal scattering angle (7°) and for the minimal energy of the scattered electron (5 GeV). From (6.2) we obtain $Q^2_{\min} \approx 2.1\,\mathrm{GeV}^2/c^2$. The maximal value of Q^2 is obtained at the largest scattering angle (178°) and maximal scattering energy (820 GeV). This yields $Q^2_{\max} = 10^5\ (\mathrm{GeV}/c)^2$. The corresponding values of x are obtained from $x = Q^2/2Pq$, where we have to substitute the four-momentum transfer q by the four-momenta of the incoming and scattered electron. This gives us $x_{\min} \approx 2.7 \cdot 10^{-5}$ and $x_{\max} \approx 1$.

(e) The transition matrix element and hence the cross-section of a reaction depend essentially upon the coupling constants and the propagator (4.23), (10.3). We have

$$\sigma_{\mathrm{em}} \propto \frac{e^2}{Q^4}\,, \qquad \sigma_{\mathrm{weak}} \propto \frac{g^2}{(Q^2 + M_{\mathrm{W}}^2 c^2)^2}\,.$$

Equating these expressions and using $e = g \sin\theta_{\mathrm{W}}$ implies that the strengths of the electromagnetic and weak interactions will be of the same order of magnitude for $Q^2 \approx M_{\mathrm{W}}^2 c^2 \approx 10^4\ \mathrm{GeV}^2/c^2$.

Chapter 9

1. (a) The relation between the event rate $\dot{N}$, the cross-section σ and the luminosity $\mathcal{L}$ is from (4.13): $\dot{N} = \sigma \cdot \mathcal{L}$. Therefore using (9.5)

$$\dot{N}_{\mu^+\mu^-} = \frac{4\pi\alpha^2\hbar^2c^2}{3 \cdot 4E^2} \cdot \mathcal{L} = 0.14/\mathrm{s}\,.$$

At this centre-of-mass energy, $\sqrt{s} = 8\,\mathrm{GeV}$, it is possible to produce pairs of u-, d-, s- and c-quarks. The ratio R defined in (9.10) can therefore be calculated using (9.11) and we so obtain $R = 10/3$. This implies

$$\dot{N}_{\mathrm{hadrons}} = \frac{10}{3} \cdot \dot{N}_{\mu^+\mu^-} = 0.46/\mathrm{s}\,.$$

(b) At $\sqrt{s} = 500\,\text{GeV}$ pair creation of all 6 quark flavours is possible. The ratio is thus $R = 5$. To reach a statistical accuracy of 10 % one would need to detect 100 events with hadronic final states. From $N_{\text{hadrons}} = 5 \cdot \sigma_{\mu^+\mu^-} \cdot \mathcal{L} \cdot t$ we obtain $\mathcal{L} = 8 \cdot 10^{33}\,\text{cm}^{-2}\,\text{s}^{-1}$. Since the cross-section falls off sharply with increasing centre-of-mass energies, future e^+e^--accelerators will need to have luminosities of an order 100 times larger than present day storage rings.

2. (a) From the supplied parameters we obtain $\delta E = 1.9\,\text{MeV}$ and thus $\delta W = \sqrt{2}\,\delta E = 2.7\,\text{MeV}$. Assuming that the natural decay width of the Υ is smaller than δW, the measured decay width, i.e., the energy dependence of the cross-section, merely reflects the uncertainty in the beam energy (and the detector resolution). This is the case here.

(b) Using $\lambda\!\!\!^{-} = \hbar/|\boldsymbol{p}| \approx (\hbar c)/E$ we may re-express (9.8) as

$$\sigma_f(W) = \frac{3\pi\hbar^2 c^2 \Gamma_{e^+e^-}\Gamma_f}{4E^2\,[(W - M_\Upsilon c^2)^2 + \Gamma^2/4]}\,.$$

In the neighbourhood of the (sharp) resonance we have $4E^2 \approx M_\Upsilon^2 c^4$. From this we obtain

$$\int \sigma_f(W)\,\mathrm{d}W = \frac{6\pi\hbar^2 c^2 \Gamma_{e^+e^-}\Gamma_f}{M_\Upsilon^2 c^4\,\Gamma}\,.$$

The measured quantity was $\int \sigma_f(W)\,\mathrm{d}W$ for $\Gamma_f = \Gamma_{\text{had}}$. Using $\Gamma_{\text{had}} = \Gamma - 3\Gamma_{\ell^+\ell^-} = 0.925\Gamma$ we find $\Gamma = 0.051\,\text{MeV}$ for the total natural decay width of the Υ. The true height of the resonance ought therefore to be $\sigma(W = M_\Upsilon) \approx 4{,}100\,\text{nb}$ (with $\Gamma_f = \Gamma$). The experimentally observed peak was, as a result of the uncertainty in the beam energy, less than this by a factor of over 100 (see Part a).

Chapter 10

1. $p + \overline{p} \to \ldots$ strong interaction.
   $p + K^- \to \ldots$ strong interaction.
   $p + \pi^- \to \ldots$ baryon number not conserved, so reaction impossible.
   $\overline{\nu}_\mu + p \to \ldots$ weak interaction, since neutrino participates.
   $\nu_e + p \to \ldots$ lepton number not conserved, so reaction impossible
   $\Sigma^0 \to \ldots$ electromagnetic interaction, since photon radiated off.
2. (a) • $\mathcal{C}|\gamma\rangle = -1|\gamma\rangle$. The photon is its own antiparticle. Its C-parity is -1 since it couples to electric charges which change their sign under the $\mathcal{C}$-parity transformation.

- $\mathcal{C}|\pi^0\rangle = +1|\pi^0\rangle$, since $\pi_0 \to 2\gamma$ and C-parity is conserved in the electromagnetic interaction.
- $\mathcal{C}|\pi^+\rangle = |\pi^-\rangle$, not a $\mathcal{C}$-eigenstate.
- $\mathcal{C}|\pi^-\rangle = |\pi^+\rangle$, not a $\mathcal{C}$-eigenstate.
- $\mathcal{C}(|\pi^+\rangle - |\pi^-\rangle) = (|\pi^-\rangle - |\pi^+\rangle) = -1(|\pi^-\rangle - |\pi^+\rangle)$, $\mathcal{C}$-eigenstate.
- $\mathcal{C}|\nu_e\rangle = |\overline{\nu}_e\rangle$, not a $\mathcal{C}$-eigenstate.
- $\mathcal{C}|\Sigma^0\rangle = |\overline{\Sigma}^0\rangle$, not a $\mathcal{C}$-eigenstate.

(b)
- $\mathcal{P}\boldsymbol{r} = -\boldsymbol{r}$
- $\mathcal{P}\boldsymbol{p} = -\boldsymbol{p}$
- $\mathcal{P}\boldsymbol{L} = \boldsymbol{L}$ since $\boldsymbol{L} = \boldsymbol{r} \times \boldsymbol{p}$
- $\mathcal{P}\boldsymbol{\sigma} = \boldsymbol{\sigma}$, since $\boldsymbol{\sigma}$ is also angular momentum;
- $\mathcal{P}\boldsymbol{E} = -\boldsymbol{E}$, positive and negative charges are (spatially) flipped by $\mathcal{P}$ the field vector thus changes its direction;
- $\mathcal{P}\boldsymbol{B} = \boldsymbol{B}$, magnetic fields are created by moving charges, the sign of the direction of motion and of the position vector are both flipped (cf. Biot-Savart law: $B \propto q\boldsymbol{r}\times\boldsymbol{v}/|\boldsymbol{r}|^3$).
- $\mathcal{P}(\boldsymbol{\sigma} \cdot \boldsymbol{E}) = -\boldsymbol{\sigma} \cdot \boldsymbol{E}$
- $\mathcal{P}(\boldsymbol{\sigma} \cdot \boldsymbol{B}) = \boldsymbol{\sigma} \cdot \boldsymbol{B}$
- $\mathcal{P}(\boldsymbol{\sigma} \cdot \boldsymbol{p}) = -\boldsymbol{\sigma} \cdot \boldsymbol{p}$
- $\mathcal{P}(\boldsymbol{\sigma} \cdot (\boldsymbol{p}_1 \times \boldsymbol{p}_2)) = \boldsymbol{\sigma} \cdot (\boldsymbol{p}_1 \times \boldsymbol{p}_2)$

3. (a) Since pions have spin 0, the spin of the f_2-meson must be transferred into orbital angular momentum for the pions, i.e., $\ell = 2$. Since $P = (-1)^\ell$, the parity of the f_2-meson is $P = (-1)^2 * P_\pi^2 = +1$. Since the parity and $\mathcal{C}$-parity transformations of the f_2-decay both lead to the same state (spatial exchange of π^+/π^- and exchange of the π-charge states) we have $C = P = +1$ for the f_2-meson.

   (b) A decay is only possible if P and C are conserved by it. Since $\mathcal{C}|\pi^0\rangle|\pi^0\rangle = +1|\pi^0\rangle|\pi^0\rangle$ and the angular momentum argument of (a) remains valid ($\ell = 2 \to P = +1$), the decay $f_2 \to \pi^0\pi^0$ is allowed. For the decay into two photons we have: $\mathcal{C}|\gamma\rangle|\gamma\rangle = +1$. The total spin of the two photons must be $2\hbar$ and the z-component $S_z = \pm 2$. Therefore one of the two photons must be left-handed and the other right-handed. (Sketch the decay in the centre-of-mass system and draw in the momenta and spins of the photons!) Only a linear combination of $S_z = +2$ and $S_z = -2$ can fulfil the requirement of parity conservation, e.g., the state $(|S_z = +2\rangle + |S_z = -2\rangle)$. Applying the parity operator to this state yields the eigenvalue $+1$. This means that the decay into two photons is also possible.

4.(a) The pion decays in the centre-of-mass frame into a charged lepton with momentum $\boldsymbol{p}$ and a neutrino with momentum $-\boldsymbol{p}$. Energy conservation supplies $m_\pi c^2 = \sqrt{m_\ell^2 c^4 + |\boldsymbol{p}|^2 c^2} + |\boldsymbol{p}|c$. For the charged lepton we have

$E_\ell^2 = m_\ell^2 c^4 + |\boldsymbol{p}|^2 c^2$. Taking $v/c = |\boldsymbol{p}|c/E_\ell$ one obtains from the above relations

$$1 - \frac{v}{c} = \frac{2m_\ell^2}{m_\pi^2 + m_\ell^2} = \begin{cases} 0.73 & \text{for } \mu^+ \\ 0.27 \cdot 10^{-4} & \text{for } \mathrm{e}^+ . \end{cases}$$

(b) The ratio of the squared matrix elements is

$$\frac{|\mathcal{M}_{\pi\mathrm{e}}|^2}{|\mathcal{M}_{\pi\mu}|^2} = \frac{1 - v_\mathrm{e}/c}{1 - v_\mu/c} = \frac{m_\mathrm{e}^2}{m_\mu^2} \frac{m_\pi^2 + m_\mu^2}{m_\pi^2 + m_\mathrm{e}^2} = 0.37 \cdot 10^{-4} .$$

(c) We need to calculate $\varrho(E_0) = \mathrm{d}n/\mathrm{d}E_0 = \mathrm{d}n/\mathrm{d}|\boldsymbol{p}| \cdot \mathrm{d}|\boldsymbol{p}|/\mathrm{d}E_0 \propto |\boldsymbol{p}|^2 \mathrm{d}|\boldsymbol{p}|/\mathrm{d}E_0$. From the energy conservation equation (see Part a) we find $\mathrm{d}|\boldsymbol{p}|/\mathrm{d}E_0 = 1 + v/c = 2m_\pi^2/(m_\pi^2 + m_\ell^2)$ and $|\boldsymbol{p}_\ell| = c(m_\pi^2 - m_\ell^2)/(2m_\pi)$. Putting it together we get

$$\frac{\varrho_\mathrm{e}(E_0)}{\varrho_\mu(E_0)} = \frac{(m_\pi^2 - m_\mathrm{e}^2)^2}{(m_\pi^2 - m_\mu^2)^2} \frac{(m_\pi^2 + m_\mathrm{e}^2)^2}{(m_\pi^2 + m_\mu^2)^2} = 3.49 .$$

Therefore the phase space factor for the decay into the positron is larger.

(d) The ratio of the partial decay widths now only depends upon the masses of the particles involved and turns out to be

$$\frac{\Gamma(\pi^+ \to \mathrm{e}^+ \nu)}{\Gamma(\pi^+ \to \mu^+ \nu)} = \frac{m_\mathrm{e}^2}{m_\mu^2} \frac{(m_\pi^2 - m_\mathrm{e}^2)^2}{(m_\pi^2 - m_\mu^2)^2} = 1.28 \cdot 10^{-4} .$$

This value is in good agreement with the experimental result.

5. (a) The decay is isotropic in the pion's centre-of-mass frame (marked by a circumflex) and we have $\hat{\boldsymbol{p}}_\mu = -\hat{\boldsymbol{p}}_\nu$. Four-momentum conservation $p_\pi^2 = (p_\mu + p_\nu)^2$ implies

$$|\hat{\boldsymbol{p}}_\mu| = \frac{m_\pi^2 - m_\mu^2}{2m_\pi} c \approx 30 \text{ MeV}/c \quad \text{and thus}$$

$$\hat{E_\mu} = \sqrt{\hat{\boldsymbol{p}}_\mu^2 c^2 + m_\mu^2 c^4} \approx 110 \text{ MeV} .$$

Using $\beta \approx 1$ and $\gamma = E_\pi/m_\pi c^2$, the Lorentz transformations of $\hat{E}_\mu$ into the laboratory frame for muons emitted in the direction of the pion's flight ("forwards") and for those emitted in the opposite direction ("backwards") are

$$E_\mu = \gamma \left(\hat{E}_\mu \pm \beta |\hat{\boldsymbol{p}}_\mu| c \right) \Longrightarrow \begin{cases} E_{\mu,\max} \approx E_\pi , \\ E_{\mu,\min} \approx E_\pi (m_\mu/m_\pi)^2 . \end{cases}$$

The muon energies are therefore: $200 \text{ GeV} \lesssim E_\mu \lesssim 350 \text{ GeV}$.

(b) In the pion centre-of-mass frame the muons are 100 % longitudinally polarised because of the parity violating nature of the decay (Sect. 10.5). This polarisation must now be transformed into the laboratory frame. Consider initially just the "forwards" decays: the pion and muon momenta are parallel to the direction of the transformation. Such a Lorentz transformation will leave the spin unaffected and we see that these muons will also be 100 % longitudinally polarised, i.e., $P_{\text{long}} = 1.0$. Similarly for decays in the "backwards" direction we have $P_{\text{long}} = -1.0$. The extremes of the muon energies thus lead to extreme values of the polarisation. If we select at intermediate muon energies we automatically vary the longitudinal polarisation of the muon beam. For example 260 GeV muon beams have $P_{\text{long}} = 0$. The general case is given in [9]. P_{long} depends upon the muon energy as

$$P_{\text{long}} = \frac{u - \left[(m_\mu^2/m_\pi^2)(1-u)\right]}{u + \left[(m_\mu^2/m_\pi^2)(1-u)\right]}, \qquad \text{where} \qquad u = \frac{E_\mu - E_{\mu,\text{min}}}{E_{\mu,\text{max}} - E_{\mu,\text{min}}}.$$

6. (a) The photon energy in the electron rest frame is obtained through a Lorentz transformation with dilatation factor $\gamma = 26.67\ \text{GeV}/m_e c^2$. This yields $E_i = 2\gamma\, E_\gamma = 251.6$ keV for $E_\gamma = 2\pi\hbar c/\lambda = 2.41$ eV.

(b) Photon scattering off a stationary electron is governed by the Compton scattering formula:

$$E_f(\theta) \;=\; \left(\frac{1-\cos\theta}{mc^2} \;+\; \frac{1}{E_i}\right)^{-1},$$

where $E_f(\theta)$ is the energy of the photon after the scattering and θ is the scattering angle. Scattering through 90° (180°) leads to $E_f = 168.8$ (126.8) keV. After the reverse transformation into the laboratory system, we have the energy E'_γ:

$$E'_\gamma(\theta) \;=\; \gamma\, E_f(\theta)\,(1-\cos\theta) \;=\; \gamma\,\left(\frac{1}{mc^2} \;+\; \frac{1}{E_i(1-\cos\theta)}\right)^{-1}.$$

For the two cases of this example, E'_γ takes on the values 8.80 (13.24) GeV. The scattering angle in the laboratory frame θ_{lab} is also 180°, i.e., the outgoing photon flies exactly in the direction of the electron beam. Generally we have

$$\theta_{\text{lab}} = \pi - \frac{1}{\gamma\ \tan\frac{\theta}{2}}.$$

(c) For $\theta = 90°$ this yields $\theta_{\text{lab}} = \pi - 1/\gamma = \pi - 19.16\ \mu$rad. The spatial resolution of the calorimeter must therefore be better than 1.22 mm.

Chapter 11

1. The neutrino flux is $\Phi_\nu = 6 \cdot 10^{10}\,\mathrm{cm}^{-2}\,\mathrm{s}^{-1}$. The number of ^{71}Ga nuclei is then

$$\begin{aligned} N_{^{71}\mathrm{Ga}} &= \frac{\text{total Gallium mass}}{\text{mean mass per atom}} \cdot \text{fraction } ^{71}\mathrm{Ga} \\ &= \frac{3 \cdot 10^4\,\mathrm{kg}}{(0.40 \cdot 71 + 0.60 \cdot 69) \cdot 931.5 \cdot 1.6 \cdot 10^{-13}\mathrm{J}/c^2} \cdot 0.40 \\ &= 1.0 \cdot 10^{29}\,, \end{aligned}$$

   from which the reaction rate can be calculated:

$$\begin{aligned} \dot{N}_{\text{reaction}} &= N_{^{71}\mathrm{Ga}} \cdot \sigma_{\nu\mathrm{Ge}} \cdot \Phi_\nu \cdot \varepsilon \\ &= 1.0 \cdot 10^{29} \cdot 2.5 \cdot 10^{-45}\,\mathrm{cm}^2 \cdot 6.0 \cdot 10^{10}\,\mathrm{cm}^{-2}\mathrm{s}^{-1} \cdot 0.5 \\ &= 0.7/\mathrm{day}\,. \end{aligned}$$

   Since $N(t) = \dot{N}_{\text{reaction}}\,\tau(1 - \mathrm{e}^{-t/\tau})$ one expects after three weeks 8 Ge atoms and after a very long time 11 atoms.
   Note: The cross-section is highly energy-dependent. The quoted value is an average one that takes into account the energy spectrum of the solar neutrinos.
2. The solutions can be easily confirmed by inserting them in the expressions. The mixing angle in matter is maximal for $\sin^2 2\theta_\mathrm{M} = 1$, or $\frac{c^4 \Delta m^2}{2E} \cos 2\theta = \sqrt{2}\,G_\mathrm{F} N_\mathrm{e}$. Remarkably this can occur for arbitrarily small, but different from zero, values of the mixing angle in vacuum, θ. Also, this resonance is only possible for $\Delta m^2 > 0$. For antineutrinos the additional term in H_M changes its sign, and the resonance can only occur for negative Δm^2. One can therefore distinguish the normal from the inverted mass ordering. Matter effects are discussed in detail in [5].
3. The CP-transformed channel is $P_{\bar{\nu}_\alpha \to \bar{\nu}_{\cdot}}$, since CP transforms left-handed neutrinos into right-handed antineutrinos. The T-transformed channel is $P_{\nu_{\cdot} \to \nu_\alpha}$. Therefore the effect of CPT is $P_{\nu_\alpha \to \nu_{\cdot}} \to P_{\bar{\nu}_\beta \to \bar{\nu}_{\cdot}}$, and since CPT is conserved it follows $P_{\nu_\alpha \to \nu_{\cdot}} = P_{\bar{\nu}_\beta \to \bar{\nu}_{\cdot}}$. Survival probabilities have $\alpha = \beta$, and hence $P_{\nu_\alpha \to \nu_{\cdot}} = P_{\bar{\nu}_\alpha \to \bar{\nu}_{\cdot}}$.
4. In case of an inverted hierarchy we have $m_2 \approx m_1 \approx \sqrt{|\Delta m^2_{31}|}$, and we can neglect $\sin^2\theta_{13}\, m_3$ with respect to the other two terms in $m_{\beta\beta}$. Thus we have

$$m_{\beta\beta} \approx \cos^2\theta_{13} \sqrt{|\Delta m^2_{31}|}\,\left|\cos^2\theta_{12} + \sin^2\theta_{12}\, e^{i\gamma}\right|\,.$$

   The minimal value occurs for $e^{i\gamma} = -1$, and is given by

$$m^{\min}_{\beta\beta} \approx \cos^2\theta_{13} \cos 2\theta_{12} \sqrt{|\Delta m^2_{31}|} \approx 0.018\,\mathrm{eV}/c^2\,.$$

We can now rule out the Majorana character of the neutrinos as follows: assume that a future neutrino oscillation experiment shows that the inverted mass ordering is realised. Hence $m_{\beta\beta}$ must be larger than $0.018\,\mathrm{eV}/c^2$. If experiments that look for neutrinoless double beta decay obtain a limit on $m_{\beta\beta}$ that is smaller than this value, neutrinos must be Dirac particles.

Chapter 12

1. The total width Γ_{tot} of Z^0 may be written as

$$\Gamma_{\mathrm{tot}} = \Gamma_{\mathrm{had}} + 3\Gamma_\ell + N_\nu \Gamma_\nu$$

and $\Gamma_\nu/\Gamma_\ell = 1.99$ (see text). From (12.9) it follows that

$$\sigma_{\mathrm{had}}^{\mathrm{max}} = \frac{12\pi(\hbar c)^2}{M_{\mathrm{Z}}^2} \frac{\Gamma_{\mathrm{e}}\Gamma_{\mathrm{had}}}{\Gamma_{\mathrm{tot}}} .$$

Solving for Γ_{tot} and inserting it into the above formula yields from the experimental results $N_\nu = 2.96$. Varying the experimental results inside the errors only changes the calculated value of N_ν by about ± 0.1 .

Chapter 14

1. The reduced mass of positronium is $m_{\mathrm{e}}/2$. From (14.4) we thus find the ground state ($n = 1$) radius to be

$$a_0 = \frac{2\hbar}{\alpha m_{\mathrm{e}} c} = 1.1 \cdot 10^{-10}\,\mathrm{m} .$$

The range of the weak force may be estimated from Heisenberg's uncertainty relation:

$$R \approx \frac{\hbar}{M_{\mathrm{W}} c} = 2.5 \cdot 10^{-3}\,\mathrm{fm} .$$

At this separation the weak and electromagnetic couplings are of the same order of magnitude. The masses of the two particles, whose bound state would have the Bohr radius R, would then be

$$M \approx \frac{2\hbar}{\alpha R c} \approx 2 \cdot 10^4\,\mathrm{GeV}/c^2 .$$

This is equivalent to the mass of $4 \cdot 10^7$ electrons or $2 \cdot 10^4$ protons. This vividly shows just how weak the weak force is.

2. From (19.1) the transition probability obeys $1/\tau \propto E_\gamma^3 |\langle r_{fi} \rangle|^2$. If m is the reduced mass of the atomic system, we have $|\langle r_{fi} \rangle| \propto 1/m$ and $E_\gamma \propto m$. $1/\tau = m/m_e \cdot 1/\tau_H$ implies $\tau = \tau_H/940$ for protonium.
3. The transition frequency in positronium $f_{e^+e^-}$ is given by

$$\frac{f_{e^+e^-}}{f_H} = \frac{7}{4} \frac{g_e}{g_p} \frac{m_p}{m_e} \frac{|\psi(0)|^2_{e^+e^-}}{|\psi(0)|^2_H} .$$

Using (14.4) one finds $|\psi(0)|^2 \propto m_{red}^3 = [(m_1 \cdot m_2)/(m_1 + m_2)]^3$. One so obtains $f_{e^+e^-} = 204.5\,\text{GHz}$. One can analogously find $f_{\mu^+e^-} = 4.579\,\text{GHz}$. The deviations from the measured values (0.5 % and 2.6 % respectively) are due to higher order QED corrections to the level splitting. These are suppressed by a factor of the order $\alpha \approx 0.007$.

Chapter 15

1. Angular momentum conservation requires $\ell = 1$, since pions are spin-0. In the ($\ell = 1$) state, the wave function is antisymmetric, but two identical bosons must have a totally symmetric wave function.
2. The branch in the denominator is Cabibbo-suppressed and from (10.21) we thus expect: $R \approx 20$.
3. (a) From the decay law $N(t) = N_0\, e^{-t/\tau}$ we obtain the fraction of the decaying particles to be $F = (N_0 - N)/N_0 = 1 - e^{-t/\tau}$. In the laboratory frame we have $t_{lab} = d/(\beta c)$ and $\tau_{lab} = \gamma\tau^*$, where τ^* is the usual lifetime in the rest frame of the particle. We thus obtain

$$F = 1 - \exp\left(-\frac{d}{\beta c \gamma \tau^*}\right) = 1 - \exp\left(-\frac{d}{\sqrt{1 - \frac{m^2c^4}{E^2}}\, c\, \frac{E}{mc^2}\, \tau^*}\right),$$

and from this we find $F_\pi = 0.9\,\%$ and $F_K = 6.7\,\%$.

(b) From four momentum conservation we obtain, e.g., for pion decay $p_\mu^2 = (p_\pi - p_\nu)^2$ and upon solving for the neutrino energy get

$$E_\nu = \frac{m_\pi^2 c^4 - m_\mu^2 c^4}{2(E_\pi - |\boldsymbol{p}_\pi| c \cos\theta)} .$$

At $\cos\theta = 1$ we have maximal E_ν, while for $\cos\theta = -1$ it is minimal. We can so obtain $E_\nu^{max} \approx 87.5\,\text{GeV}$ and $E_\nu^{min} \approx 0\,\text{GeV}$ (more precisely: 11 keV)

in pion decay. In the case of kaon decay, we obtain $E_\nu^{\max} \approx 191\,\text{GeV}$ and $E_\nu^{\min} \approx 0\,\text{GeV}$ (more precisely: 291 keV).

4. (a) The average decay length is $s = v\tau_{\text{lab}} = c\beta\gamma\tau$ where $\gamma = E_\text{B}/m_\text{B}c^2 = 0.5\,m_\Upsilon/m_\text{B}$ and $\beta\gamma = \sqrt{\gamma^2 - 1}$. One thus obtains $s = 0.028\,\text{mm}$.
   (b) From $0.2\,\text{mm} = c\beta\gamma\tau = \tau \cdot |\boldsymbol{p}_\text{B}|/m_\text{B}$ we obtain $|\boldsymbol{p}_\text{B}| = 2.3\,\text{GeV}/c$.
   (c) From the assumption, $m_\text{B} = 5.29\,\text{GeV}/c^2 = m_\Upsilon/2$, the B-mesons do not have any momentum in the centre-of-mass frame. In the laboratory frame, $|\boldsymbol{p}_\text{B}| = 2.3\,\text{GeV}/c$ and thus $|\boldsymbol{p}_\Upsilon| = 2|\boldsymbol{p}_\text{B}|$. We obtain from this $E_\Upsilon = \sqrt{m_\Upsilon^2 c^4 + \boldsymbol{p}_\Upsilon^2 c^4} = 11.6\,\text{GeV}$.
   (d) From four-momentum conservation $p_\Upsilon = p_{\text{e}^+} + p_{\text{e}^-}$ we obtain (setting $m_\text{e} = 0$) $E_\Upsilon = E_{\text{e}^+} + E_{\text{e}^-}$ and $\boldsymbol{p}_\Upsilon\, c = E_{\text{e}^+} + E_{\text{e}^-}$ from this we get $E_{\text{e}^+} = 8.12\,\text{GeV}$ and $E_{\text{e}^-} = 3.44\,\text{GeV}$ (or vice-versa).

Chapter 16

1. (b) All of the neutral mesons made out of u- and d-quarks (and similarly the $\text{s}\bar{\text{s}}$ (ϕ) meson) are very short lived; $c\tau < 100\,\text{nm}$. The dilatation factor γ that they would need to have in order to traverse a distance of several centimetres in the laboratory frame is simply not available at these beam energies. Since mesons with heavy quarks (c, b) cannot be produced, as not enough energy is available, the only possible mesonic decay candidate is the K^0_S. Similarly the only baryons that come into question are the Λ^0 and the $\overline{\Lambda}^0$. The primary decay modes of these particles are $\text{K}^0_\text{S} \to \pi^+\pi^-$, $\Lambda^0 \to \text{p}\pi^-$ and $\overline{\Lambda}^0 \to \overline{\text{p}}\pi^+$.
   (c) We have for the mass M_X of the decayed particle from (16.1)

$$M_\text{X}^2 = m_+^2 + m_-^2 + 2\sqrt{\boldsymbol{p}_+^2/c^2 + m_+^2}\sqrt{\boldsymbol{p}_-^2/c^2 + m_-^2} - \tfrac{2}{c^2}|\boldsymbol{p}_+||\boldsymbol{p}_-|\cos\sphericalangle(\boldsymbol{p}_+, \boldsymbol{p}_-)\,,$$

   where the masses and momenta of the decay products are denoted by $m_\pm$ and $\boldsymbol{p}_\pm$ respectively. Consider the first pair of decay products: the hypothesis that we have a $\text{K}^0_\text{S} \to \pi^+\pi^-$ ($m_\pm = m_{\pi\pm}$) decay leads to $M_\text{X} = 0.32\,\text{GeV}/c^2$ which is inconsistent with the true K^0 mass ($0.498\,\text{GeV}/c^2$). The hypothesis $\Lambda^0 \to \text{p}\pi^-$ ($m_+ = m_\text{p}$, $m_- = m_{\pi^-}$) leads to $M_\text{X} = 1.11\,\text{GeV}/c^2$ which is in very good agreement with the mass of the Λ^0. The $\overline{\Lambda}^0$ possibility can, as with the K^0 hypothesis, be confidently excluded. Considering the second pair of decay particles we similarly find: K^0 hypothesis, $M_\text{X} = 0.49\,\text{GeV}/c^2$; Λ^0 hypothesis, $M_\text{X} = 2.0\,\text{GeV}/c^2$; the $\overline{\Lambda}^0$ hypothesis also leads to a contradiction. In this case we are dealing with the decay of a K^0.
   (d) Conservation of strangeness in the strong interaction means that as well as the Λ^0, which is made up of a uds quark combination, a further hadron with an $\bar{\text{s}}$-quark must be produced. The observed K^0_S decay means that this was

a K^0 ($\bar{s}d$).[1] Charge and baryon number conservation now combine to imply that the most likely total reaction was

$$p + p \to K^0 + \Lambda^0 + p + \pi^+ .$$

We cannot, however, exclude additional, unobserved neutral particles or very short lived intermediate states (such as a Δ^{++}).

2. Let us consider the positively charged Σ particles $|\Sigma^+\rangle = |u^\uparrow u^\uparrow s^\downarrow\rangle$ and $|\Sigma^{+*}\rangle = |u^\uparrow u^\uparrow s^\uparrow\rangle$. Since the spins of the two u-quarks are parallel, we have

$$\sum_{\substack{i,j=1\\ i<j}}^{3} \frac{\boldsymbol{\sigma}_i \cdot \boldsymbol{\sigma}_j}{m_i m_j} = \frac{\boldsymbol{\sigma}_u \cdot \boldsymbol{\sigma}_u}{m_u^2} + 2\,\frac{\boldsymbol{\sigma}_u \cdot \boldsymbol{\sigma}_s}{m_u m_s} .$$

We first inspect

$$2\,\boldsymbol{\sigma}_u \cdot \boldsymbol{\sigma}_s = \sum_{\substack{i,j=1\\ i<j}}^{3} \boldsymbol{\sigma}_i \cdot \boldsymbol{\sigma}_j - \boldsymbol{\sigma}_u \cdot \boldsymbol{\sigma}_u .$$

We already know the first term on the r.h.s. from (16.10). It is -3 for $S = 1/2$ baryons and $+3$ for $S = 3/2$ baryons. The second term is $+1$. This yields

$$\Delta M_{ss} = \begin{cases} \dfrac{4}{9}\dfrac{\hbar^3}{c^3}\pi\alpha_s\,|\psi(0)|^2\left(\dfrac{1}{m_{u,d}^2} - \dfrac{4}{m_{u,d}m_s}\right) & \text{for the } \Sigma \text{ states,} \\ \dfrac{4}{9}\dfrac{\hbar^3}{c^3}\pi\alpha_s\,|\psi(0)|^2\left(\dfrac{1}{m_{u,d}^2} + \dfrac{2}{m_{u,d}m_s}\right) & \text{for the } \Sigma^* \text{ states.} \end{cases}$$

The average mass difference between the Σ and Σ^* baryons is about $200\,\mathrm{MeV}/c^2$. With the mass formula (16.12) we have

$$\begin{aligned} M_{\Sigma^*} - M_\Sigma &= \Delta M_{ss}(\Sigma^*) - \Delta M_{ss}(\Sigma) = \tfrac{4}{9}\tfrac{\hbar^3}{c^3}\pi\alpha_s\,|\psi(0)|^2\,\tfrac{6}{m_{u,d}m_s} \\ &\approx 200\,\mathrm{MeV}/c^2 , \end{aligned}$$

where we assume that $\psi(0)$ is the same for both states. We thus obtain ($m_{u,d} = 363\,\mathrm{MeV}/c^2$, $m_s = 538\,\mathrm{MeV}/c^2$)

$$\alpha_s\,|\psi(0)|^2 = 0.61\,\mathrm{fm}^{-3} .$$

[1] Both the K^0 and the $\overline{K}^0$ can decay as K^0_S (cf. Sect. 15.4).

Inserting a hydrogen atom-type wave function, $|\psi(0)|^2 = 3/4\pi r^3$, and $\alpha_s \approx 1$, yields a rough approximation for the average separation r of the quarks in such baryons: $r \approx 0.8\,\mathrm{fm}$.

3. The Λ is an isospin singlet ($I = 0$). To a first approximation the decay is just the quark transition s $\to$ u, which changes the isospin by 1/2. Thus the pion-nucleon system must be a $I = 1/2$ state. Charge conservation implies that the third component is $I_3^{\mathrm{N}} + I_3^{\pi} = -1/2$. The matrix elements of the decay of the Λ^0 are proportional to the squares of the Clebsch-Gordan coefficients:

$$\frac{\sigma(\Lambda^0 \to \pi^- + \mathrm{p})}{\sigma(\Lambda^0 \to \pi^0 + \mathrm{n})} = \frac{(1\ \frac{1}{2}\ -1\ +\frac{1}{2}\ |\ \frac{1}{2}\ -\frac{1}{2})^2}{(1\ \frac{1}{2}\ 0\ -\frac{1}{2}\ |\ \frac{1}{2}\ -\frac{1}{2})^2} = \frac{(-\sqrt{2/3})^2}{(\sqrt{1/3})^2} = 2.$$

4. The probability that a muon be captured from a 1s state into a ^{12}C nucleus is

$$\frac{1}{\tau_{\mu\mathrm{C}}} = \frac{2\pi}{\hbar}\left|\left\langle {}^{12}\mathrm{B}\,\mathrm{e}^{ip_\nu r}\right| \sum_i g_{\mathrm{A}}\boldsymbol{\sigma}_i I_- \left|{}^{12}\mathrm{C}\psi_\mu(r)\right\rangle_{(r=0)}\right|^2 \int \frac{p_\nu^2 \mathrm{d}p_\nu \mathrm{d}\Omega}{(2\pi\hbar)^3 \mathrm{d}E_\nu}\,.$$

Since carbon has $J^P = 0^+$ and boron $J^P = 1^+$, this is a purely axial vector transition. We further have $\mathrm{d}p_\nu/\mathrm{d}E_\nu = 1/c$, $\int \mathrm{d}\Omega = 4\pi$ and $\left|\psi_\mu(r=0)\right|^2 = 3/(4\pi r_\mu^3)$. The radius of the ^{12}C muonic atomic is found to be

$$r_\mu = \frac{a_{\mathrm{Bohr}} m_{\mathrm{e}}}{Z m_\mu} = 42.3\,\mathrm{fm}\,,$$

and the energy is

$$E_\nu = m_\mu c^2 - 13.3\,\mathrm{MeV} \approx 90\,\mathrm{MeV}\,.$$

This yields the absorption probability

$$\frac{1}{\tau_{\mu\mathrm{C}}} = \frac{2\pi}{\hbar c}\frac{4\pi c E_\nu^2}{(2\pi)^3(\hbar c)^3}\left|\left\langle {}^{12}\mathrm{B}\right| \sum_i g_{\mathrm{A}}\boldsymbol{\sigma}_i I_- \left|{}^{12}\mathrm{C}\right\rangle\right|^2 |\psi(0)|^2\,.$$

These are all known quantities except for the matrix element. This may be extracted from the known lifetime of the $^{12}\mathrm{B} \to {}^{12}\mathrm{C} + \mathrm{e}^- + \overline{\nu}_{\mathrm{e}}$ decay:

$$\frac{1}{\tau_{^{12}\mathrm{B}}} = \frac{1}{2\pi^3\hbar^7 c^6}\left|\left\langle {}^{12}\mathrm{C}\right| \sum_i g_{\mathrm{A}}\boldsymbol{\sigma}_i I_+ \left|{}^{12}\mathrm{B}\right\rangle\right|^2 E_{\max}^5\,.$$

We thus finally obtain

$$\frac{1}{\tau_{\mu\mathrm{C}}} \approx 1.5 \cdot 10^4\,\mathrm{s}^{-1}\,.$$

The total decay probability of the muon decay in ^{12}C is the sum of the probabilities of the free muon decaying and of its being captured by the nucleus:

$$\frac{1}{\tau} = \frac{1}{\tau_\mu} + \frac{1}{\tau_{\mu\mathrm{C}}} .$$

5. These branching ratios depend primarily upon two things: (a) the phase space and (b) the fact that the strangeness changes in the first case (Cabibbo suppression) but not in the latter. A rough estimate may be obtained by assuming that the matrix elements are, apart from Cabibbo suppression, identical. From (10.21) and (16.58) one finds

$$\frac{W(\Sigma^- \to \mathrm{n})}{W(\Sigma^- \to \Lambda^0)} \approx \frac{\sin^2\theta_\mathrm{C}}{\cos^2\theta_\mathrm{C}} \cdot \left(\frac{E_1}{E_2}\right)^5 = \frac{1}{20} \cdot \left(\frac{257\,\mathrm{MeV}}{81\,\mathrm{MeV}}\right)^5 \approx 16 .$$

This agreement is not bad at all, considering the coarseness of our approximation. In the decay $\Sigma^+ \to n + e^+ + \nu_e$ we would need two quarks to change their flavours; (suu) $\to$ (ddu).

6. (a) Baryon number conservation means that baryons can neither be annihilated nor created but rather only transformed into each other. Hence only the relative parities of the baryons have any physical meaning.
   (b) The deuteron is a ground state p-n system, i.e., $\ell = 0$. Its parity is therefore $\eta_\mathrm{d} = \eta_\mathrm{p}\eta_\mathrm{n}(-1)^0 = +1$. Since quarks have zero orbital angular momentum in nucleons, the quark intrinsic parities must be positive.
   (c) The downwards cascade of pions into the ground state may be seen from the characteristic X-rays.
   (d) Since the deuteron has spin 1, the d-π system is in a state with total angular momentum $J = 1$. The two final state neutrons are identical fermions and so must have an antisymmetric spin-orbit wave function. Only $^3\mathrm{P}_1$ of the four possible states with $J = 1$, $^3\mathrm{S}_1$, $^1\mathrm{P}_1$, $^3\mathrm{P}_1$ and $^3\mathrm{D}_1$ fulfils this requirement.
   (e) From $\ell_{nn} = 1$, we see that the pion parity must be $\eta_\pi = \eta_\mathrm{n}^2(-1)^1/\eta_\mathrm{d} = -1$.
   (f) The number of quarks of each individual flavour ($N_\mathrm{q} - N_{\bar{\mathrm{q}}}$) is separately conserved in parity conserving interactions. The quark parities can therefore be separately chosen. One could thus choose, e.g., $\eta_\mathrm{u} = -1, \eta_\mathrm{d} = +1$, giving the proton a positive and the neutron a negative parity. The deuteron would then have a negative parity and the charged pions a positive one. The π^0 as a $\mathrm{u\bar{u}}/\mathrm{d\bar{d}}$ mixed state would though keep its negative parity. Particles like (π^+, π^0, π^-) or (p, n) although inside the same isospin multiplets would then have distinct parities – a rather unhelpful convention. For $\eta_\mathrm{n} = \eta_\mathrm{p} = -1$, on the other hand, isospin symmetry would be fulfilled. The parities of nucleons and odd nuclei would then be the opposite of the standard convention, while those of mesons and even nuclei would be unchanged. The Λ and Λ_c parities are just those of the s- and c-quarks and may be chosen to be positive.

Chapter 17

1. The ranges, $\lambda \approx \hbar c/mc^2$, are: 1.4 fm ($1\pi$), 0.7 fm ($2\pi$), 0.3 fm ($\varrho$, ω). Two pion exchange with vacuum quantum numbers, $J^P = 0^+, I = 0$, generates a scalar potential which is responsible for nuclear binding. Because of its negative parity, the pion is emitted with an angular momentum, $\ell = 1$. The spin dependence of this component of the nuclear force is determined by this. Similar properties hold for the ϱ and ω. The isospin dependence is determined by the isospin of the exchange particle; $I = 1$ for the π and ϱ and $I = 0$ for the ω. Since isospin is conserved in the strong interaction, the isospin of interacting particles is coupled, just as is the case with angular momentum.
2. Taking (17.1), (17.2) and (17.6) into account we obtain

$$\sigma = 4\pi \left(\frac{\sin kb}{k} \right)^2 .$$

At low energies, where the $\ell = 0$ partial wave dominates, we obtain in the $k \to 0$ limit, the total cross-section, $\sigma = 4\pi b^2$.

Chapter 18

1. At constant entropy S the pressure obeys

$$p = -\left(\frac{\partial U}{\partial V} \right)_S ,$$

where V is the volume and U is the internal energy of the system. In the Fermi gas model we have from (18.9):

$$U = \frac{3}{5} A E_\mathrm{F} \qquad \text{and hence} \qquad p = -\frac{3}{5} A \frac{\partial E_\mathrm{F}}{\partial V} .$$

From (18.3) we find for $N = Z = A/2$:

$$A = 2\frac{V p_\mathrm{F}^3}{3\pi^2\hbar^3} = 2\frac{V(2ME_\mathrm{F})^{3/2}}{3\pi^2\hbar^3} \quad \Longrightarrow \quad \frac{\partial E_\mathrm{F}}{\partial V} = -\frac{2E_\mathrm{F}}{3V} .$$

The Fermi pressure is then

$$p = \frac{2A}{5V} E_\mathrm{F} = \frac{2}{5} \varrho_\mathrm{N} E_\mathrm{F} ,$$

where ϱ_N is the nucleon density. This implies for $\varrho_N = 0.17$ nucleons/fm^3 and $E_F \approx 33\,\text{MeV}$

$$p = 2.2\,\text{MeV/fm}^3 = 3.6 \cdot 10^{27}\,\text{bar}\,.$$

2. (a) We only consider the odd nucleons. The even ones are all paired off in the ground state. The first excited state is produced either by (I) the excitation of the unpaired nucleon into the next subshell or (II) by the pairing of this nucleon with another which is excited from a lower lying subshell.

	$^{7}_{3}$Li	$^{23}_{11}$Na	$^{33}_{16}$S	$^{41}_{21}$Sc	$^{83}_{36}$Kr	$^{93}_{41}$Nb
Ground state	$1p^1_{3/2}$	$1d^3_{5/2}$	$1d^1_{3/2}$	$1f^1_{7/2}$	$1g^{-3}_{9/2}$	$1g^1_{9/2}$
Excited (I)	$1p^1_{1/2}$	$2s^1_{1/2}$	$(1f^1_{7/2})$	$(2p^1_{3/2})$	$(1g^1_{7/2})$	$(1g^1_{7/2})$
Excited (II)	$(1s^{-1}_{1/2})$	$1p^{-1}_{1/2}$	$2s^{-1}_{1/2}$	$1d^{-1}_{3/2}$	$2p^{-1}_{1/2}$	$2p^{-1}_{1/2}$
J^P_0 experiment	$3/2^-$	$3/2^+$	$3/2^+$	$7/2^-$	$9/2^+$	$9/2^+$
J^P_0 model	$3/2^-$	$5/2^+$	$3/2^+$	$7/2^-$	$9/2^+$	$9/2^+$
J^P_1 experiment	$1/2^-$	$5/2^+$	$1/2^+$	$3/2^+$	$7/2^+$	$1/2^-$
J^P_1 case (I)	$1/2^-$	$1/2^+$	$(7/2^-)$	$(3/2^-)$	$(7/2^+)$	$(7/2^+)$
J^P_1 case (II)	$(1/2^+)$	$1/2^-$	$1/2^+$	$3/2^+$	$1/2^-$	$1/2^-$

Those states whose excitation would be beyond a "magic" boundary are shown here in brackets. This requires a lot of energy and so is only to be expected for higher excitations. As one sees, the predictive powers of the shell model are good for those nuclei where the unfilled subshell is only occupied by a single nucleon.

(b) The $(p - 1p^1_{3/2}; n - 1p^1_{3/2})$ in $^{6}_{3}$Li implies $J^P = 0^+, 1^+, 2^+, 3^+$. $^{40}_{19}$K has from $(p - 1d^{-1}_{3/2}; n - 1f^1_{7/2})$ a possible coupling to$2^-, 3^-, 4^-, 5^-$.

3. (a) An ^{17}O nucleus may be viewed as being an ^{16}O nucleus with an additional neutron in the $1f_{5/2}$ shell. The energy of this level is thus $B(^{16}\text{O}) - B(^{17}\text{O})$. The $1p_{1/2}$ shell is correspondingly at $B(^{15}\text{O}) - B(^{16}\text{O})$. The gap between the shells is thus

$$E(1f_{5/2}) - E(1p_{1/2}) \;=\; 2B(^{16}\text{O}) - B(^{15}\text{O}) - B(^{17}\text{O}) = 11.5\,\text{MeV}\,.$$

(b) One would expect the lowest excitation level with the "right" quantum numbers to be produced by exciting a nucleon from the topmost, occupied shell into the one above. For ^{16}O this would be the $J^P = 3^-$ state, which is at 6.13 MeV, and could be interpreted as $(1p^{-1}_{1/2}, 1d_{5/2})$. The excitation energy is, however, significantly smaller than the theoretical result of 11.5 MeV. It seems that collective effects (state mixing) are making themselves felt. This is confirmed by the octupole radiation transition probability, which is an order of magnitude above what one would expect for a single particle excitation.

(c) The $1/2^+$ quantum numbers make it natural to interpret the first excited state of ^{17}O as $2s_{1/2}$. The excitation energy is then the gap between the shells.

(d) Assuming (more than a little naively) that the nuclei are homogeneous spheres with identical radii, one finds from (2.11) that the difference in the

binding energies implies the radius is $(3/5) \cdot 16\hbar\alpha c/3.54\,\text{MeV} = 3.90$ fm, which is much larger than the value of 3.1 fm, which follows from (5.56). In the shell model one may interpret each of these nuclei as an ^{16}O nucleus with an additional nucleon. The valence nucleon in the $d_{5/2}$ shell thus has a larger radius than one would expect from the above simple formula which does not take shell effects into account.

(e) The larger Coulomb repulsion means that the potential well felt by the protons in ^{17}F is shallower than that of the neutrons in ^{17}O. As a result the wave function of the excited, "additional" proton in ^{17}F is more spread out than that of the equivalent "additional" neutron in ^{17}O and the nuclear force felt by the neutron is stronger than that acting upon the proton. This difference is negligible for the ground state since the nucleon is more strongly bound.

4. At the upper edge of the closed shells which correspond to the magic numbers 50 and 82 we find the closely adjacent $2p_{1/2}$, $1g_{9/2}$ and the $2d_{3/2}$, $1h_{11/2}$, $3s_{1/2}$ levels respectively. It is thus natural that for nuclei with nucleon numbers just below 50 or 82 the transition between the ground state and the first excited state is a single particle transition ($g_{9/2} \leftrightarrow p_{1/2}$ and $h_{11/2} \leftrightarrow d_{3/2}, s_{1/2}$ respectively). Such processes are 5th order (M4 or E5) and hence extremely unlikely [6].
5. (a) The spin of the state is given by the combination of the unpaired nucleons which are in the $(p - 1f_{7/2},\ n - 1f_{7/2})$ state.

   (b) The nuclear magnetic moment is just the sum of the magnetic moments of the neutron in the $f_{7/2}$ shell $-1.91\ \mu_N$ and of the proton in the $f_{7/2}$ shell $+5.58\ \mu_N$. From (18.36) we would expect a g factor of 1.1.
6. (a) In the de-excitation $i \to f$ of an Sm nucleus *at rest* the atom receives a recoil energy of $\boldsymbol{p}_{\text{Sm}}^2/2M$ where $|\boldsymbol{p}_{\text{Sm}}| = |\boldsymbol{p}_\gamma| \approx (E_i - E_f)/c$. In the case at hand this is 3.3 eV. The same amount of energy is lost when the photon is absorbed by another Sm nucleus.

   (b) If we set the matrix element in (19.1) to one, this implies a lifetime of $\tau = 0.008$ ps, which is equivalent to $\Gamma = 80$ MeV. In actual measurements one finds $\tau = 0.03$ ps, i.e., $\Gamma = 20$ MeV [10], which is of a similar size. Since the width of the state is much smaller than the energy shift of $2 \cdot 3.3$ eV, no absorption can take place. Thermal motion will change $|\boldsymbol{p}_{\text{Sm}}|$ by roughly $\pm\sqrt{M \cdot kT}$. At room temperature this corresponds to smearing the energy by ± 0.35 eV, which is also insufficient.

   (c) If the Sm atom emits a neutrino before the deexcitation, then $|\boldsymbol{p}_{\text{Sm}}|$ is changed by $\pm|\boldsymbol{p}_\nu| = \pm E_\nu/c$. If the emission directions of the neutrino and of the photon are opposite to each other, then the energy of the radiated photon is 3.12 eV larger than the excitation energy $E_i - E_f$. This corresponds to the classical Doppler effect. In this case resonant fluorescence is possible for the γ radiation. The momentum direction of the neutrino can be determined in this fashion.
7. The three lowest proton shells in the ^{14}O nucleus, the $1s_{1/2}$, $1p_{3/2}$ and $1p_{1/2}$, are fully occupied as are the two lowest neutron shells. The $1p_{1/2}$ shell is, however, empty (sketched on p. 333). Thus one of the two valence nucleons (one of

the protons in their $1p_{1/2}$ shell) can transform into a neutron at the equivalent level and with the same wave function (super allowed β-decay). We thus have $\int \psi_n^* \psi_p = 1$. This is a $0^+ \to 0^+$ transition, i.e., a pure Fermi decay. Each of the two protons contributes a term to the matrix element equal to the vector part of (16.48). The total is therefore $|\mathcal{M}_{fi}|^2 = 2g_V^2/V^2$. Equation (16.56) now becomes

$$\frac{\ln 2}{t_{1/2}} = \frac{1}{\tau} = \frac{m_e^5 c^4}{2\pi^3 \hbar^7} \cdot 2g_V^2 \cdot f(E_0)\,.$$

Using the vectorial coupling (16.65) one finds the half-life is 70.373 s – which is remarkably close to the experimental value. Note: the quantum numbers and definite shell structure here means that this is one of the few cases where a nuclear β-decay can be calculated exactly. In practice this decay is used to determine the strength of the vectorial coupling.

Chapter 19

1. (a) In the collective model of giant resonances we consider Z protons and N neutrons whose mutual vibrations are described by a harmonic oscillator. The Hamiltonian may be written as

$$\mathcal{H} = \frac{p^2}{2m} + \frac{m\omega^2}{2}x^2\,, \qquad \text{where} \qquad \hbar\omega = 80\,A^{-1/3}\,\text{MeV}\,,$$

and $m = A/2M_N$ is the reduced mass. The solution of the Schrödinger equation yields the lowest lying oscillator states [14]

$$\psi_0 = \frac{1}{\sqrt[4]{\pi}\sqrt{x_0}} \cdot e^{-(x/x_0)^2/2}\,, \qquad \text{where} \quad x_0 = \sqrt{\hbar/m\omega}\,,$$

$$\psi_1 = \frac{1}{\sqrt[4]{\pi}\sqrt{x_0}} \cdot \sqrt{2}\left(\frac{x}{x_0}\right) e^{-(x/x_0)^2/2}\,.$$

The average deviation is

$$x_{01} := \langle\psi_0|x|\psi_1\rangle = \frac{\sqrt{2}}{\sqrt{\pi}}x_0 \int \left(\frac{x}{x_0}\right)^2 e^{-(x/x_0)^2}\,\mathrm{d}\frac{x}{x_0} = \frac{\sqrt{2}}{\sqrt{\pi}}x_0\,.$$

For ^{40}Ca we have $x_0 = 0.3$ fm and $x_{01} = 0.24$ fm.

(b) The matrix element is Zx_{01}. Its square is therefore 23 fm^2.

(c) The single particle excitations have about half the energy of the giant resonance, i.e., $\hbar\omega \approx 40A^{-1/3}$MeV. The reduced mass in this case is approximately the nucleon mass, since the nucleon moves in the mean field

of the heavy nucleus. This increases x_0, and thus x_{01}, by a factor of $\sqrt{40}$. The 24 nucleons in the outermost shell each contribute to the square of the matrix element with an effective charge $e/2$. The square of the matrix element is so seen to be 27.6 fm^2. The agreement with the result of (b), i.e., the model where the protons and neutrons oscillate collectively, is very good.

2. Using the definitions in Chap. 18.4, we obtain for small deformations

$$\varepsilon \approx \frac{3}{2} \cdot \frac{a-b}{\langle R \rangle}, \ \langle R \rangle = (ab^2)^{1/3} .$$

(a) From this we get $a = (1+\varepsilon)\langle R \rangle$, $b = \langle R \rangle / \sqrt{1+\varepsilon} \approx (1-\varepsilon/2)\langle R \rangle$ and $Q = \frac{6}{5} Ze \langle R \rangle^2 \varepsilon$. With the central nuclear density $\varrho_{\mathrm{N}} \approx 0.17$ nucleons/fm^3 (5.59), we obtain $a \approx 7.6$ fm, $b \approx 5.7$ fm, $Q \approx 710 \cdot e$ fm^2. The nucleus is prolately deformed.

(b) For a rotation of a rigid ellipsoid transverse to its symmetry axis, the moment of inertia is

$$\Theta_{\text{rigid ellipsoid}} = \frac{1}{5} M(a^2 + b^2) .$$

For small deformations we have

$$\Theta_{\text{rigid ellipsoid}} \approx (1 + \frac{\varepsilon}{2} + \varepsilon^2) \cdot \Theta_{\text{rigid sphere}},$$

and we obtain $\Theta_{\text{rigid ellipsoid}} \approx 1.15 \cdot \Theta_{\text{rigid sphere}}$, with $\Theta_{\text{rigid sphere}} = \frac{2}{5} M \langle R \rangle^2 \approx 2.6 \cdot 10^6 \, \mathrm{MeV}/c^2 \, \mathrm{fm}^2$ being the moment of inertia of a rigid sphere.

If the nucleus would behave as an ideal fluid, then it would have a moment of inertia $\Theta_{\text{ideal fluid}} \approx 0.086 \cdot \Theta_{\text{rigid sphere}} \approx 2.2 \cdot 10^5 \, \mathrm{MeV}/c^2 \, \mathrm{fm}^2$.

3. The Fermi velocity is $v_{\mathrm{F}} = p_{\mathrm{F}} / \sqrt{M_{\mathrm{N}}^2 + p_{\mathrm{F}}^2/c^2} = 0.26\, c$. The angular velocity is

$$\omega = \frac{|\boldsymbol{L}|}{\Theta} \approx \frac{60\hbar}{A M_{\mathrm{N}} (a^2 + b^2)^2 / 5} = 0.95 \cdot 10^{21} \, \mathrm{s}^{-1} ,$$

where $a = 2b = \sqrt[3]{4} R$, and we have employed the value of R from (5.56). The speed is $v = a \cdot \omega$ and is about 0.03 c or around 12 % of the Fermi velocity. The high rotational velocity causes a Coriolis force which is responsible for breaking up the nucleon pairs.

Chapter 20

1. (a) In the reaction $4\mathrm{p} \rightarrow \alpha + \mathrm{e}^+ + 2\nu_\mathrm{e}$, 26.72 MeV of energy is released. The neutrinos carry off 0.52 MeV, and so 26.2 MeV remains to heat up the Sun. The number of hydrogen atoms which are converted into helium every second is:

$$\dot{N}_\mathrm{p} = 4 \cdot \frac{4 \cdot 10^{26}\,\mathrm{W}}{26.4 \times 1.6 \cdot 10^{-13}\,\mathrm{Ws}} \approx 0.4 \cdot 10^{39}\,\mathrm{atoms/s}\,.$$

   (b) $0.4 \cdot 10^{10}\,\mathrm{kg/s}$
   (c) $\approx 7\,\%$
   (d) $\approx$ 130 terrestrial masses
   (e) Nuclear reactions take place in the interior of the Sun, primarily at radii $r < R_\odot/4$. By burning off 7 % of the hydrogen the helium concentration in the interior of the Sun is increased by about 50 %. Doubling this concentration means that hydrogen burning is no longer efficient: helium burning starts up and the Sun swells into a red giant.
2. (a) The number of neutrons in the neutron star is $N_\mathrm{n} = 1.8 \cdot 10^{57}$. The energy released by fusing N_n protons into ^{56}Fe is $2.6 \cdot 10^{45}$ J.
   (b) We neglect the gravitational energy of the iron core in the original star, (since $R \gg 10\,\mathrm{km}$). Thus the energy released during the implosion is the gravitational energy of the neutron star minus the energy needed to transform the iron into free neutrons (this last is the energy which was originally released during the fusion of hydrogen into iron):

$$E_\mathrm{Implosion} \approx \frac{3GM^2}{5R} - 2.6 \cdot 10^{45}\,\mathrm{J} = 3.3 \cdot 10^{46}\,\mathrm{J}\,.$$

   The energy released via the implosion during the supernova explosion is more than ten times larger than the fusion energy. Although only about 20-50 % of the matter of the original star ends up in the neutron star, the fusion energy released during the entire lifetime of the star is slightly less than the energy released in the supernova explosion.
   (c) Most of the energy is radiated off as neutrino emission:

$$\mathrm{e}^+ + \mathrm{e}^- \rightarrow \overline{\nu}_\mathrm{e} + \nu_\mathrm{e}, \overline{\nu}_\mu + \nu_\mu, \overline{\nu}_\tau + \nu_\tau.$$

   The positrons in this process are generated in the reaction:

$$\mathrm{p} + \overline{\nu}_\mathrm{e} \rightarrow \mathrm{e}^+ + \mathrm{n}\,.$$

Neutrinos can, however, also be directly produced in:

$$\mathrm{p} + \mathrm{e}^- \rightarrow \mathrm{n} + \nu_\mathrm{e}\,.$$

The last two processes are responsible for the transformation of the protons in ^{56}Fe.

References

1. H.A. Bethe, Ann. Physik **5**, 325 (1930)
2. F. Bloch, Ann. Physik **16**, 285 (1933)
3. E.R. Cohen, B.N. Taylor, Rev. Mod. Phys. **59**, 1121 (1987)
4. T. Ferbel, *Experimental Techniques in High Energy Physics* (Addison-Wesley, Menlo Park, 1987)
5. C. Giunti, C.W. Kim, *Fundamentals of Neutrino Physics and Astrophysics* (Oxford University Press, Oxford, 2007)
6. M. Goldhaber, A.W. Sunyar, Phys. Rev. **83**, 906 (1951)
7. C. Grupen, B.A. Schwarz, *Particle Detectors*, 2nd edn. (Cambridge University Press, Cambridge, 2008)
8. P. Langacker, in *Precision Tests of the Standard Electroweak Model*, ed. by P. Langacker (World Scientific, Singapur, 1995)
9. L.M. Lederman, M.J. Tannenbaum, in *Advances in Particle Physics*, ed. by R.L. Cool, R.E. Marshak, vol. 1 (Interscience, New York, 1968)
10. C.M. Lederer, V.S. Shirley, *Table of Isotopes*, 7th edn. (Wiley, New York, 1978)
11. W.R. Leo, *Techniques for Nuclear and Particle Physics Experiments*, 2nd edn. (Springer, Berlin/Heidelberg/New York, 1994)
12. Particle Data Group, J. Beringer et al., *Review of Particle Properties*. Phys. Rev. D **86**, 010001 (2012)
13. P.W. Petley, Nature **303**, 373 (1983)
14. F. Schwabl, *Quantum Mechanics*, 4th edn. (Springer, Berlin/Heidelberg/New York, 2007)
15. K. Wille, *The Physics of Particle Accelerators* (Oxford University Press, Oxford, 2000)
16. E. Wilson, E.J.N. Wilson, *An Introduction to Particle Accelerators* (Oxford University Press, Oxford, 2001)
17. H. Wiedemann, *Particle Accelerator Physics*, 3rd edn. (Springer, Berlin/Heidelberg/New York, 2007)

Index

Absorption coefficient, 413
Activity, 26
Alpha decay, 25, 31
Antiproton, 186
Asymmetry
  energy, 20, 306
  term, 20
Asymptotic freedom, 110, 222
ATLAS experiment, 202
Atomic number, 13
Axial vector current, 155, 280, 331

BaBar experiment, 154, 245, 248
Baryon, 103, 104, 253–255
  number conservation, 104
Beauty oscillations, 245, 249
Belle experiment, 154, 245, 248
Beta decay, 25, 27–29, 274–277, 281, 330, 332
  allowed, 332
  double, 29, 338
  forbidden, 332
  inverse, 144, 307
  neutrinoless double, 180, 340
  super allowed, 332
Bethe-Bloch formula, 412
Bhabha scattering, 127
Big bang, 204
Binding energy, 19, 20, 25, 294, 305, 306, 310, 311
  of deuteron, 17, 292–294
  of hypernuclei, 310
Bjorken scaling variable, 89
Bohr magneton, 423
Bohr radius, 216, 217, 423
Born approximation, 59, 325, 326
Boson
  gluons, 3, 4
  Goldstone, 198
  Higgs particle, 197–200, 202
  photon, 3, 4
  W, 3, 4, 143, 144, 146, 187
  Z^0, 3, 4, 123, 133, 143, 186, 187, 189
Bottonium, 226
  decays, 229
Breit frame, 94, 119
Breit-Wigner formula, 129, 190
Bremsstrahlung, 412
Bubble chamber, 414

C-Parity, 5, 156
Cabibbo angle, 152, 276
Cabibbo-Kobayashi-Maskawa matrix, see CKM matrix, 153
Callan-Gross relation, 92
Calorimeter, 416
Carbon cycle, 396
Central potential, 292, 312
CERN, 42, 87, 186, 187, 410
Chaos, 401, 402
Charge
  colour, 4, 104–106, 108
  conjugation, 5, 156
  distribution, 67, 70, 80
  electric, 4
  weak, 4, 146, 147
Charge radius, 70
  of kaons, 85
  of neutron, 81

B. Povh et al., *Particles and Nuclei*, Graduate Texts in Physics,
DOI 10.1007/978-3-662-46321-5

of nuclei, 71
of pions, 85
of proton, 79, 80
Charmonium, 218–220
Cherenkov counter, 419
Cherenkov radiation, 173, 414
Chiral perturbation theory, 300
Chirality, 154
Chromomagnetic interaction, 225, 226, 263, 297
CKM matrix, 153, 246
Wolfenstein parametrisation, 246
Clebsch-Gordan coefficients, 262, 421, 422
CLEO experiment, 154
COBE satellite, 386
Colour, 104–106, 133–135, 151
wave function, 260
Compound nucleus, 378
Compact Muon Solenoid (CMS) experiment, 202
Compton effect, 413
Confinement, 106, 110, 222
Conservation laws, 208
Constituent quarks, 108, 226, 233, 270, 282, 402
Cooper pairs, 197, 199, 370
Coriolis force, 449
Coulomb
barrier, 32
excitation, 364, 365
potential, 31, 215
term, 20, 34
threshold, 364
Coupling constant
electromagnetic, 7, 108, 109, 216
strong, 106, 109, 115, 135, 137
weak, 147, 151, 192
Covalent bond, 298, 402
CP violation, 153, 157, 244–247, 249
in B^0 decays, 247, 249
CKM matrix, 246
direct, 244
in K^0 decays, 244
indirect, 244
Critical density, 386
Cross-section, 44
differential, 48
geometric, 45
total, 46
Crystal ball, 219
Current quarks, 108

Dark energy, 386
Dark matter, 386
Daya Bay experiment, 177
De Broglie wavelength, 43
Decay
chain, 33
constant, 26
width, 129
Deformation, 35, 320, 321, 323, 369, 370
Delayed neutron emission, 334
Δ resonance, 89, 253, 254, 260
Deuteron, 97, 292
binding energy, 17, 292–294
dipole moment, 293
magnetic moment, 292, 293
quadrupole moment, 292
Deutsche Elektronen-Synchrotron (DESY), 42, 87, 410, 411
DGLAP equations, 113, 114
Dipole
form factor, 78
oscillator, 351ff
transition, electric, 36, 219, 350
transition, magnetic, 36, 220
Dirac particle, 180, 266
Direct nuclear reaction, 324
Distorted-wave Born approximation (DWBA), 328
Doppler shift, 385
Double beta decay, 338
neutrinoless, 180, 340
Double Chooz experiment, 177
Drell-Yan process, 116
Drift chamber, 414
DWBA. *See* Distorted-wave Born approximation (DWBA)

Electron
capture, 29
charge, 11, 13
discovery, 11
magnetic moment, 76
mass, 12, 14
volt, 6
EMC effect, 117, 118, 297
Exclusive measurement, 44

Fermi
constant, 146, 147, 275
decay, 275, 331

energy, 305
function, 330
gas, 84, 303, 304
momentum, 84, 304, 307, 310
motion, 83, 97
pressure, 308
Feynman diagrams, 50
Fine structure, 216, 217
Fine structure constant, 7
Flavour, 96, 143
Flux, 44
FNAL, 42, 87, 133
Form factor, 61, 64, 66, 67, 80, 81
dipole, 78
electric, 77, 80
of kaons, 85
magnetic, 77, 80
monopole, 85
of neutron, 77, 80
of nuclei, 66–68
of nucleons, 81
of pions, 85
of proton, 77
Formation experiments, 255
Four-momentum, 55, 56
transfer, 75, 76
Four-vector, 55
Friedman model, 386
ft value, 331
Fusion reactions, 368

g-factor, 76
of electron, 76
of neutron, 77
of nuclei, 319
of proton, 77
G-parity, 240
Gamma decay, 36–38
Gamow factor, 32, 33
Gamow-Teller decay, 276, 331–333
Gauss system, 7
Giant dipole resonance, 38, 347, 348, 352, 353, 359
Gluon, 101, 105–108, 119, 135, 137
distribution, 114, 116–118
Golden rule, 49, 50, 147, 275, 325
Goldhaber experiment, 337
Gottfried sum rule, 100, 116
Grand unified theory (GUT), 204
Gravitational Doppler shift, 307

H1 detector, 110
H1 experiment, 110, 112, 162, 193
Hadronic matter, 381, 383
Hadronisation, 134, 136, 224
Hadrons, 103
Half life, 26
Hard core, 290, 308
Heavyside-Lorentz system, 7
Helicity, 63, 154, 156, 271
HERA, 42, 87, 161, 272, 410, 411
HERMES experiment, 272
Higgs boson, 197, 198, 200, 202
mass, 200–203
production, 201, 202
Higgs potential, 197
Hubble constant, 385
Hund rule, 322
Hyperfine structure, 216, 217, 319
Hypernuclei, 308, 309
Hyperon, 253, 255, 308
magnetic moment, 268
semileptonic decays, 280, 281

Impulse approximation, 82, 93
Inclusive measurement, 44
Internal conversion, 37, 38
Invariant mass, 257, 258
Ionisation, 412, 414, 416
Isobars, 14
Isomers, 38
Isospin, 5, 22, 234, 288
strong, 5, 275
weak, 5, 274, 276
Isotones, 14
Isotopes, 14

Jacobian peak, 188
Jets, 136
JLab, 79

K capture, 29, 144, 333, 337
KamLAND detector, 177
Kaon, 85, 131, 239
K_S^0 regeneration, 243
charge radius, 85
KATRIN experiment, 180
Klein-Gordon equation, 299
Kurie plot, 335

Large Electron Positron (LEP), 41, 133, 185, 410
Large Hadron Collider (LHC), 42, 199, 202

Larmor frequency, 269
Leptogenesis, 390
Lepton, 125, 126, 128, 141
  families, 141, 168
  family number, 142
  number, 142
  number conservation, 142
  number violation, 181
  universality, 128
Leptonic processes, 144
Lifetime, 26, 31, 38
Linear accelerator, 406
Liquid drop model, 20
log-*ft* value, 331
Luminosity, 47

Magic numbers, 313, 314
Magnetic moment, 76
  of deuteron, 292
  of electron, 76
  of hyperons, 268
  of neutron, 76
  of nuclei, 318, 319
  of nucleons, 76, 266, 267
  of proton, 76
  in the quark model, 266
Magnetic spectrometer, 64, 416
Majorana neutrino, 180, 340, 390
Mass
  defect, 13
  formula, 19, 306
  invariant, 56
  number, 14
Meissner effect, 196, 197, 199
Meson(s), 103, 104, 233–235
  B, 230
  D, 229
  exchange of, 298
  Υ, 133, 226, 229
  J/ψ, 132, 218, 228–231
  pseudoscalar, 234, 236
  vector, 130
Mirror nuclei, 21, 316, 317
Moment of inertia, 363, 365, 368–370
Momentum transfer, 60–62, 67, 76
Moseley's law, 13
Mott cross-section, 63, 75
Muon, 139
  beam, 87
  decay, 140, 147, 155
  experiments, 161
  lifetime, 147

Neutrino, 140–142
  atmospheric, 175
  electron-, 141
  experiments, 161
  helicity, 155, 156, 337, 338
  mass, 167, 178, 180, 335, 336, 342, 390
  mass ordering, 176, 178
  mass-squared difference, 175, 176
  muon-, 141
  oscillations, 167, 168, 171
  reactor, 176
  scattering, 157, 158
  solar, 171
  tau-, 141
Neutron
  capture, 17, 35, 38
  charge radius, 81
  decay, 275, 278, 279
  lifetime, 279
  magnetic moment, 77, 267
  mass, 14
  scattering, 38
  star, 307, 308
Nilsson model, 323
Non-leptonic processes, 145
Nuclear
  fission (*see* Nuclear fission)
  force, 287–289
  magneton, 77, 266, 423
  matter, 373, 374
  photoelectric effect, 38, 352
  spin resonance, 319
  temperature, 374
Nuclear fission
  barrier, 34, 35
  induced, 35
  spontaneous, 25, 34
Nucleon resonances, 88, 254
Nuclides, 14

Oscillations
  beauty-, 245, 249
  neutrino, 167, 168, 171, 175, 176, 178
  strangeness-, 243

Pair production, 413
Pairing
  force, 322, 370
  term, 20, 21
Parity, 5, 314, 332
  intrinsic, 5, 234
  of nuclear levels, 314

of quarkonia, 219
violation, 154–157
Partial waves, 288, 289
Partial width, 129
Parton distributions, 116
Parton model, 93, 96–98, 100
Phase space, 49
Phase transition, electroweak, 390
Photoelectric effect, 413
Pick-up reaction, 328
Pion, 85, 104, 239, 310
charge radius, 85
decay, 141, 156
parity, 240
Pions, 298
Planck constant, 7
Planck experiment, 386
PMNS matrix, 168
Point interaction, 146–148, 225
Poisson equation, 299
Polarisation experiments, 81, 161, 272
Polarised beams, 81, 161, 271
Polarised targets, 81, 272
Pontecorvo, 168
Positronium, 215, 217
Potential well, 304, 305
Principal quantum number, 215, 218
Probability amplitude, 48
Production experiments, 255, 280
Propagator, 52, 62, 146
Proportional counter, 414
Proton
anti-, 186
charge, 13
charge radius, 79
decay, 104
magnetic moment, 77, 266
mass, 14
Proton-proton cycle, 395

Quadrupole moment
of deuteron, 292, 293
of nuclei, 320, 321
Quadrupole oscillations, 360, 361
Quadrupole transition, 36, 351
Quantum chaos, 374
Quantum chromodynamics, 50, 87, 105–107, 109, 221
Quantum electrodynamics, 50, 55
Quark, 95, 96
charge, 95, 100
distribution, 96, 114, 116–118
families, 96
helicity distributions, 271
isospin, 95
mass, 96, 133
matter, 308
sea quark, 96, 98, 119
spin, 95
top, 133
Quark-gluon plasma, 384, 390, 391
Quarkonia, 215
Quasi-particles, 401, 402

r-process, 399
Radiation length, 413
Recoil polarisation, 80
Renormalisation, 193
Resonances, 88, 129, 255
Resonant absorption, 337
Rosenbluth formula, 77
Rotational bands, 363, 365–368, 370
Rutherford scattering, 12
cross-section, 58

s-process, 398
s-waves, 289
Sampling calorimeter, 417
Sargent's rule, 278, 280
Scaling violations, 110, 112–115
Scattering
angle, 57
deep-inelastic, 92, 157, 158, 161
elastic, 42, 58–61
experiments, 41
inelastic, 43, 72, 88, 89
neutrino-electron, 192
of neutrinos, 157, 158
of neutrons, 376
phase, 288–290
polarised, 80, 81
quasi-elastic, 82, 403
Rutherford, 12
Scintillator, 416, 417, 419
Sea quark, 96, 98, 160, 186
Seesaw mechanism, 182
Self similarity, 116
Semiconductor detector, 416
Semileptonic processes, 144
Separation energy, 38, 310
Shadowing, 120
Shell model, 303, 312–314, 403
Silicon strip detector, 415
Spark chamber, 414
Spin dependence, of nuclear force, 292

Spin structure functions, 271
Spin structure of the nucleon, 270
Spin-orbit interaction, 216, 292, 320
Spin-spin interaction, 237, 263, 296
Splitting function, 114
Spontaneous symmetry breaking, 196
Standard model, 207, 208, 210
Stanford Linear Accelerator Center (SLAC), 79, 87, 91
Stanford Linear Collider (SLC), 185
Storage ring, 110, 123, 410
Strange particles, 131
Strangeness, 131, 234, 253
Strangeness oscillations, 243
Streamer chamber, 414
Stripping reaction, 324, 326
Structure function, 90, 91, 96
  of the deuteron, 97, 100, 111
  of the neutron, 97, 98, 100
  nuclear effects, 117–119
  polarised, 271
  of the proton, 97, 98, 100, 112
Sudbury Neutrino Observatory (SNO) experiment, 173
Superconductivity, 196, 197, 199, 370
Superfluidity, 369, 370
SuperKamiokande experiment, 173, 175
Supernova, 398
Surface term, 20, 34
Surface thickness, 71
Symmetry breaking, 197
Synchrotron, 408
  radiation, 409

Tau lepton, 126, 140
  decay, 140, 144, 151
Tensor force, 292, 293
Tevatron, 42
Thomson model, 12
Top quark, 133, 227
Transition matrix element, 48
Transition radiation detector, 419
Transmission, 32
Transverse mass, 188
Transverse momentum, 187
Tunnel effect, 32, 34

Unitarity triangle, 247, 249, 250
Universe
  closed, 386
  critical density, 386
  flat, 386
  open, 386

V−A theory, 155, 274
Vacuum expectation value, 198
Valence nucleon, 317, 330
Valence quark, 95, 96, 160, 186
Van de Graaff accelerator, 406
Van der Waals force, 298, 402
Vector current, 155, 280, 331
Vector meson, 130, 234–236
Vertex, 51
Virtual particles, 51
Volume term, 19, 20

Weak interaction
  charged currents, 143–145, 157, 162, 173, 193
  neutral currents, 143, 150, 174, 193
Weak isospin, 191
Weinberg angle, 192
Weizsäcker formula, 19
White dwarf, 308, 396, 397
WMAP experiment, 386
Woods-Saxon potential, 314

Yukawa potential, 298, 299

ZEUS detector, 419
ZEUS experiment, 110, 112, 162
Zweig rule, 132, 229, 240